

Journal of Materials Chemistry B

Accepted Manuscript



This is an *Accepted Manuscript*, which has been through the Royal Society of Chemistry peer review process and has been accepted for publication.

Accepted Manuscripts are published online shortly after acceptance, before technical editing, formatting and proof reading. Using this free service, authors can make their results available to the community, in citable form, before we publish the edited article. We will replace this *Accepted Manuscript* with the edited and formatted *Advance Article* as soon as it is available.

You can find more information about *Accepted Manuscripts* in the [Information for Authors](#).

Please note that technical editing may introduce minor changes to the text and/or graphics, which may alter content. The journal's standard [Terms & Conditions](#) and the [Ethical guidelines](#) still apply. In no event shall the Royal Society of Chemistry be held responsible for any errors or omissions in this *Accepted Manuscript* or any consequences arising from the use of any information it contains.

Magnetic field assisted stem cell differentiation - role of substrate magnetization in osteogenesis

Sunil Kumar Boda¹ ‡, Greeshma Thrivikraman^{1,3} ‡ and Bikramjit Basu^{1,2*}

¹Laboratory for Biomaterials, Materials Research Centre, ²Interdisciplinary Bio-Engineering Program, Indian Institute of Science, Bangalore – 560012

³Centre for Nano Science and Engineering, Indian Institute of Science, Bangalore - 560012

*Corresponding author e-mail: bikram@mrc.iisc.ernet.in

Abstract

Among the multiple modulatory physical cues explored to regulate cellular processes, the potential of magneto-responsive substrates in magnetic field stimulated stem cell differentiation is still unperceived. In this regard, the present work is a comprehensive effort to understand how external magnetic field can be applied to direct stem cell differentiation towards osteogenic commitment. A new culture methodology involving periodic delivery of 100 mT static magnetic field (SMF) in combination with HA-Fe₃O₄ magnetic substrates possessing varying degree of substrate magnetization was designed for the study. The results demonstrate that an appropriate combination of weakly ferromagnetic substrate and SMF exposure enhanced cell viability, DNA synthesis and caused an early switch over to osteogenic lineage as supported by Runx2 immunocytochemistry and ALP expression. However, the mRNA expression profile of early osteogenic markers (Runx2, ALP, Col IA) was comparable despite varying substrate magnetic property (diamagnetic to ferromagnetic). On the contrary, a remarkable upregulation of late bone development markers (OCN and OPN) were explicitly detected on weak and strongly ferromagnetic substrates. Furthermore, SMF induced matrix mineralization with elevated calcium deposition on similar substrates, even in the absence of osteogenic supplements. More specifically, the role of SMF in increasing intracellular calcium levels and in inducing cell cycle arrest at G0/G1 phase was elucidated as the major molecular event triggering osteogenic differentiation. Taken together, the above results demonstrate the competence of magnetic stimuli in combination with magneto-responsive biomaterials as a potential strategy for stem cell based bone tissue engineering.

Keywords: Human mesenchymal stem cells (hMSCs), static magnetic field (SMF), osteogenic, ferromagnetic

‡ These authors contributed equally

1. Introduction

It is well reported that physical cues in the form of mechanical¹, electrical² and chemical³ signals can stimulate desired cellular responses, opening up myriad opportunities to manipulate the cell fate processes of mesenchymal stem cells (MSCs). Of late, magnetic stimulation via static or pulse electromagnetic fields have been proved to accelerate bone repair during delayed fracture reunion. In particular, pulse electromagnetic fields have been reported to treat bone disorders such as bone fracture healing⁴, pseudoarthrosis^{4,5}, healing of osteotomies⁶⁻⁸ and osteoporosis.^{9, 10} by enhancing the proliferation and differentiation of osteoblasts in cell monolayers¹¹ and 3-D constructs.¹² However, *in vitro* studies to comprehensively establish the influence of external magnetic field stimulation on stem cells, when grown on magnetoactive biomaterial substrates is not yet demonstrated.

Hydroxyapatite (HA) is an obvious choice for a bone replacement material due to its excellent osseointegration with native bone tissue.¹³ However, reports of HA actively promoting the differentiation of progenitor cells into osteoblasts are not known. In earlier studies, the addition of a secondary magnetic phase or Fe doping of HA were illustrated to enhance osteoblast expression of progenitor cells (osteosarcoma, rabbit adipose tissue derived stem cells) in such HA-based magnetic composites.¹⁴⁻¹⁶ In parallel, the approach of magnetic field stimulation is also being explored to induce bone formation by osteoblasts. The magnetic stimulation of cells can be deployed to induce mechanical stresses through the binding of magnetic nanoparticles capped with ligands that bind to specific receptors on the cell surface. For example, when cultured on fibronectin and RGD peptides, it was possible to induce Col IA expression in MSCs by nanomagnetic actuation resulting from the activation of specific mechanosensitive ion-channels.^{17, 18} The repetitive collision of magnetic beads with osteoblast cells through the application of pulse magnetic field (1MHz frequency) was also shown to accelerate cell growth without any significant loss in viability and the effect was more profound, when the cells were in the G1 phase.¹⁹ A dose-dependent increase in the ALP activity and calcium mineralization of human osteoblasts in HA coated magnetite particles,²⁰ was reported with a concomitant increase in the adsorption of fibronectin.²¹ Another group demonstrated that nanoparticles of Fe-doped HA increased SaOS2 human osteoblast activity, which was further enhanced by the application of 320 mT static magnetic field.²²

It is evident that most of the earlier literature pertaining to cell response on magnetic biomaterials was carried out on HA-coated magnetite particles, nanocomposites of hydroxyapatite (HA)-iron oxide and magnetized HA with the objective of using such particles as injectable gels that can set quickly and harden to form bone tissue. Moreover, Alkaline phosphatase (ALP) activity and collagen were the only markers evaluated for osteogenesis in such studies. However, we present a detailed analysis on the effect of SMF and substrate magnetization on a host of bone development markers including Runx2, Osteocalcin (OCN) and Osteopontin (OPN) in addition to ALP and Col1A. With the perspective of manipulating cellular response to achieve desired magnetobiological effects on cells *in vitro*, the current work demonstrates how intermittent delivery of static magnetic field (100 mT) stimulus and magnetic properties of HA- $x\text{Fe}_3\text{O}_4$ biocomposites can be coupled for the osteogenic differentiation of hMSCs, when cultured without the aid of osteogenic supplements. It is worthwhile to mention that our recent work has established synergistic interaction of 100 mT SMF and magnetoactive substrate properties towards *in vitro* bactericidal properties of both gram-positive and gram-negative bacteria.²³ In our earlier research, we have attempted to understand how the intermittent electrical stimulation and/or substrate conductivity can influence the cell functionality on biomaterial substrates *in vitro*.²⁴⁻²⁷ It is therefore of interest to check how intermittent magnetic stimulation and variable magneto-responsive substrates guide stem cell differentiation.

2. Materials and Methods

2.1 Biomaterial substrate fabrication

Hydroxyapatite (HA) was synthesized from calcium oxide and phosphoric acid precursors via the suspension precipitation route as described elsewhere.²⁶ In brief, 0.17 M H_3PO_4 was added dropwise to CaO dispersed in water at a concentration of 18.6 g/L and stirred on a magnetic hot plate, at 80 °C for 3-4 h. Subsequently, concentrated NH_4OH was added drop-wise until the pH of the solution reached 10. The product was allowed to precipitate from the reaction mixture at room temperature for 24 h followed by filtration. The synthesized powders were calcined at 800 °C and ball-milled to obtain fine powders. Magnetite (Fe_3O_4)/ Iron (II, III) oxide powder with particle size < 50 nm (TEM) was purchased from Sigma Aldrich (> 98% Cat.No. 637106). The above two powders were mixed to obtain various compositions of HA- $x\text{Fe}_3\text{O}_4$, where $x = 5, 10, 20$ and 40 wt% of Fe_3O_4 and the corresponding samples were designated as HA5Fe, HA10Fe, HA20Fe and HA40Fe. The ball-milling was carried out for 16 h in a planetary ball mill (Fritsch

Pulveristee, Germany) with a ball (agate) to powder ratio of 4:1. After ball-milling in ethanol, the resultant powder slurry was dried in a hot air oven at 100 °C. The dry powders were mixed well in an agate mortar and pestle and then used for hot-pressing. The consolidation of the powders in different compositions was carried out in 10 mm graphite die using an induction furnace in Argon atmosphere. The sintering conditions used were 950 °C, 70 MPa with a holding time of 6 min. The bulk density of the sintered pellets was determined by Archimedes method using DI water.

2.2 Material characterization

2.2.1 Phase assemblage

The characterization of the phase assemblage in the sintered pellets was carried out using XRD (X'Pert Pro PaNalytical, Netherlands), operated at 40 kV and 30 mA with a Cu K α (1.5418Å) radiation. The scans were carried out at a scan rate of 1.5°/ min with a step size of 0.025° and 2 θ varying between 20-80°. The phases present were identified with the help of International Centre for diffraction data (ICDD) standard. Rietveld refinement of the XRD data, recorded at a much slower scan rate of 0.15°/ min was carried out to identify the specific phase compositions. The details of the analysis are discussed in a separate paper (unpublished work).

2.2.2 Microstructure characterization

Transmission electron microscopy was used to examine the finer microstructure of the sintered specimen. The sintered sample was polished using emery paper up to ~ 200 μ m thickness. TEM lamella with dimensions of 10 μ m x 4 μ m and 100 nm thickness was prepared using UHR dual beam Focused ion beam system (FIB, Helios NanoLab 600i, FEI). In brief, a thin Platinum wire was deposited over the polished sample and etched with a gallium ion beam at 30 kV to make a trench with above dimensions. After etching at the bottom and lift off from the bulk specimen, the lamella was welded onto a TEM copper half grid and ion milled to 100 nm thickness. STEM detector attached to the FIB enabled the milled specimen to be examined for electron transparency. The TEM lamella was desiccated under vacuum until examination under a TEM. Tecnai F30 transmission electron microscope, operated at an accelerating voltage of 300 kV was used to examine the microstructure and phases present in the magnetic lamella. In the imaging mode, bright field images of the sample were acquired to identify the phase contrast in the microstructure and selected area diffraction patterns (SADP) were acquired in the diffraction

mode. HRTEM of the different grains were also captured to identify the phases present. Gatan Digital micrograph software was used for the analysis of the TEM data.

2.2.3 Magnetic characterization

Lake Shore Vibrating sample magnetometer (VSM) was used to measure the magnetic properties of the sintered samples. For each composite, room temperature measurements gave values of saturation magnetization (M_s in emu/g), remnant magnetization (M_r in emu/g), coercive field (H_c in Gauss) and area under the hysteresis loops as a function of applied magnetic field up to a maximum of 10,000 G.

2.2.4 Surface wettability

The surface hydrophilicity/ hydrophobicity of the hot-pressed HA- $x\text{Fe}_3\text{O}_4$ composites was studied by measuring the contact angle using the sessile water drop method with distilled water. The contact angle measurements were facilitated by a goniometer (Dataphysis, Germany) coupled with a CCD camera for recording the video clippings during the measurement. 2 μL of distilled water was injected onto the polished sample surfaces with a syringe and video clippings were recorded during the measurement. For determining the contact angle values, the frame corresponding to the equilibrium state of the water droplet upon contact with the material surface was used.

2.3 *In vitro* cell culture studies

The cylindrical shaped dense pellets of 10 mm diameter and ~ 1.5 mm thickness were used for the cell culture studies. The polished samples were steam sterilized, washed with ethanol and 1X PBS (Phosphate buffered saline), before cell seeding. An in-house designed static magnetic field set up was used for the magnetic stimulation of cells on magnetic substrates *in vitro*. The details of the equipment used for magnetic field generation has been reported in one of the earlier works from our group.²⁸ In brief, it consists of a cavity of 17 cm x 15 cm x 4 cm dimensions, around which the coil was wound into a solenoid with 875 turns using a copper wire of 1.5 mm diameter. The coil was connected to a 15 V DC power source and the field generated was proportional to the electric current (DC) passing through the coil. The static magnetic field set up used for the experiments is represented in **Fig. 1A**. The magnetic field strength was measured experimentally using a GM08 Gaussmeter (Hirst magnetic Instruments Ltd, USA).

2.3.1 hMSC culture and viability

Human mesenchymal stem cells (hMSCs) were procured from Institute for Regenerative medicine, Texas A&M HSC COM and the present study was carried out after prior approval from Institute committee for stem cell research and regenerative technologies (IC-SCRT), IISc, Bangalore. The cells were revived from cryopreserved stock and grown in complete growth medium containing α -MEM (Alpha modified Eagle's medium; Invitrogen), 20% MSC-FBS (Fetal bovine serum; Invitrogen), 1% antibiotic antimycotic solution (Sigma) and 2 mM L-glutamine (Invitrogen). The cells were maintained in a CO₂ incubator (Sanyo, MCO-18AC, USA) at 37°C, 95% humidity and 5% CO₂. Upon reaching 70-80% confluency, the cells were detached from the culture flask with 0.05% Trypsin-EDTA (Invitrogen) and harvested by neutralizing with complete media after detachment and centrifugation at 425 xg for 5 min. The cells were sub-cultured for further use as required.

For assessing the viability of hMSCs, $\sim 10^4$ cells were seeded on each of HA-xFe₃O₄ composites and exposed regularly to static magnetic field of 100 mT for 30 min following the protocol shown in **Fig. 1B**. For 100 mT static magnetic field (SMF) exposure, the samples were incubated in HEPES (2-[4-(2-hydroxyethyl)piperazin-1-yl]ethanesulfonic acid) buffered complete growth medium in order to maintain neutral pH, as the stimulation was performed in an incubator without CO₂ supply. After the exposure cycle, 150 μ L of MTT (3(4,5-dimethylthiazol-2-yl)-2,5-diphenyltetrazolium bromide; Sigma) was added to the samples and incubated for 4 h. The purple colored formazan crystals formed by the reduction of MTT reagent by mitochondrial dehydrogenase was solubilized in DMSO (Merck) and the optical density was read at 595 nm using a microplate reader (Biorad).

It may be noted that the samples have been represented as HA, HA5Fe, HA10Fe, HA20Fe and HA40Fe for different sample compositions of hydroxyapatite and magnetite (without magnetic stimulation), and the suffix MF has been added for magnetic field (MF) treated samples as HA_MF, HA5Fe_MF, and so on.

2.3.2 LIVE/DEAD assay

For the LIVE/DEAD (viability/ cytotoxicity) assay, the hMSCs cultured on various HA-xFe₃O₄ composites were intermittently exposed to SMF on alternate days for one week. The live/dead staining for the samples was performed using a combination of Fluorescein diacetate (FDA) and

Propidium iodide (PI) for the live cells and dead cells, respectively. In brief, the samples were washed in 1X PBS, stained with 1 mL of 25 $\mu\text{g}/\text{mL}$ of FDA for 15 min at 37 $^{\circ}\text{C}$. Subsequently, the samples were stained with 1 mL of 10 $\mu\text{g}/\text{mL}$ of PI for 5 min at room temperature. Post-staining, the samples were washed twice with 1X PBS and visualized under Nikon Fluorescence microscope within the next 15-20 min.

2.3.3 Cell Proliferation assay

The cell proliferation was assessed by the total DNA content of the cells cultured on different samples under normal and SMF culture. The total DNA content was quantified using Quanti-iT PicoGreen dsDNA assay kit (Invitrogen), following the manufacturer's protocol. After 3, 5 and 7 days of hMSC culture, the samples were washed in 1X PBS and lysed with 250 μL of 0.1% Triton-X for 20 min. To 50 μL of the cell lysate, equal volume of 1X TE buffer and 100 μL of PicoGreen working reagent (1:300 dilution of the stock) were added to a 96 well plate. After incubation for 5 min, the fluorescence intensities were recorded using a multi-mode plate reader (Eppendorf AF2200) with excitation and emission wavelengths of 485 and 535 nm, respectively. The amounts of DNA were calculated from a standard curve of dsDNA (ng/mL) concentration and fluorescence intensity.

2.3.4 Cellular events/processes at the onset of hMSC differentiation

2.3.4.1 Cell cycle analysis

At the stage of early hMSC differentiation, the distribution of cell populations in different stages of cell cycle was investigated. The protocol followed is based on the univariate analysis of DNA content by flow cytometry after staining with Propidium iodide.²⁹ The DNA frequency histograms were deconvoluted to identify the percentage of cells in different stages of cell cycle (G0/G1 - interphase, S - synthesis and G2/M - mitotic/ dividing phase). In brief, the 7 day SMF cultured cells adhered on HA, HA10Fe and HA40Fe samples were trypsinized and harvested by centrifugation at 425 xg for 5 min. The cell pellets were washed and suspended in 1X PBS, followed by overnight fixation in 70% EtOH (ice cold) at 4 $^{\circ}\text{C}$. Subsequently, the fixed cells were washed and resuspended in staining buffer consisting of 0.1% (v/v) Triton-X, 10 $\mu\text{g}/\text{mL}$ PI (Propidium iodide, Invitrogen) and 100 $\mu\text{g}/\text{mL}$ DNase-free RNase (Invitrogen) in PBS. The samples were incubated in the staining buffer for 10 min at 37 $^{\circ}\text{C}$ and run on BD FACS CantoII

flow cytometer. A minimum of 10,000 events were acquired per sample. The data were analyzed and fit using Modfit LT4.1 software.

2.3.4.2 Intracellular calcium estimation by Fluo-4 AM

Intracellular calcium is known to control numerous cellular processes including cell division, gene regulation and cell death (apoptosis).^{30, 31} High intracellular calcium has also been implicated in the growth and differentiation of osteoblasts.³² Hence, the relative change in intracellular calcium (as compared to control) of hMSCs after 7 days of SMF culture was determined by flow cytometry. Fluo-4 AM is a non-toxic fluorescent probe (λ_{ex} : 494 nm; λ_{em} : 516 nm) specific for intracellular calcium detection. The dye is deesterified by cellular esterases and the binding of intracellular calcium to the deesterified product leads to a 100 fold increase in fluorescence intensity. The cell staining protocol was applied according to the manufacturer's instructions. Briefly, the 7 day cultured hMSCs on HA, HA10Fe and HA40Fe under SMF exposure were harvested by trypsinization and centrifugation at 425 xg for 5 min. The cell pellets were washed and suspended in HEPES buffer containing 5 mM KCl, 0.01 mM $[\text{Ca}^{2+}]$ and 0.01 mM $[\text{Mg}^{2+}]$. The cells were stained with Fluo-4 AM (Invitrogen) at a final concentration of 2 μM along with 0.1% Pluronic F-127 as the loading detergent in 1 mL of HEPES buffer. The samples were incubated at 37 °C for 30 min followed by centrifugation at 425 xg for 5 min. The stained cells were resuspended in HEPES buffer as above and run on BD FACS Canto II flow cytometer. Around 10,000 events were acquired per sample and the data was analyzed by BD FACS Diva Version 6.1.1 and an overlay of histograms was constructed using Cell quest Pro software.

2.3.5 Differentiation of hMSCs

2.3.5.1 Immunofluorescent staining with Runx2

Following the hints of differentiation of hMSCs, the expression of Runx2 expression which is an early osteogenic marker was checked by immunocytochemistry. After 5 days of SMF culture on magnetic composites, the cells were fixed with 4% paraformaldehyde (PFA) for 30 min. For immunostaining, the cells were permeabilized with 0.1% Triton-X in PBS for 5 min and 1% BSA was used for 30 min to block non-specific staining of antibodies. The primary antibody labeling with mouse anti-Runx2 (ab76956) was performed by incubating in 1:200 dilution of antibody in dilution buffer (1% BSA + 0.01% Triton-X in PBS) at room temperature for 1 h.

After washing thrice, secondary antibody labeling was performed similarly with 1:500 anti-mouse Alexa-488 FITC-conjugate. The nuclei were stained with DAPI (Invitrogen) and the cytoskeleton with Alexa Fluor 546 C5 maleimide conjugate (Invitrogen). Immunofluorescence microscopy was performed under Nikon LV100 fluorescence microscope having bandpass filters required for the fluorophores.

2.3.5.2 Alkaline phosphatase (ALP) activity

ALP activity is a well-known phenotypic biochemical marker for differentiation towards osteogenic lineage.³³ The early osteogenic differentiation of hMSCs was characterized by monitoring the enzymatic activity of alkaline phosphatase (ALP) after 7 and 14 days of culture. After the stipulated culture duration, the cells were lysed by incubation at room temperature with 300 μL of cell lysis buffer (Sigma), followed by one freeze thaw cycle between $-80\text{ }^{\circ}\text{C}$ and $37\text{ }^{\circ}\text{C}$, each at 10 min interval. 50 μL of the cell lysate was used to estimate the total cellular protein on each sample using quantipro BCA assay kit (Sigma: QPBCA), following the recommended protocol and the absorbance was measured at 595 nm. Another 50 μL of the cell lysate was used to determine the alkaline phosphatase activity using 175 μL of p-Nitrophenyl phosphate (pNPP Sigma) substrate. Following this, the absorbance measurements were immediately made at 415 nm in the kinetic cycle mode, with a regular time interval of 15 min between successive measurements. The ALP activity in IU/L or $\mu\text{mol}/(\text{L min})$ was calculated using the following equation:

$$\text{ALP activity} = [(\text{OD}_t - \text{OD}_{t=0}) \times 1000 \times \text{reaction volume}] / (t \times \epsilon \times l \times \text{sample volume})$$

where t is the time interval in min, $\epsilon = 18.75\text{ mM}^{-1}\text{ cm}^{-1}$ is the molar extinction coefficient for p-Nitrophenol and l is the path length. The ALP activity was finally quantified by normalizing to the total protein obtained from BCA assay and expressed as ($\mu\text{mol}/\text{min}$) per mg of total protein.

2.3.5.3 Sircol Collagen assay

Collagen is the major component of the extracellular matrix in bone. The Sircol dye test is based on the colorimetric estimation of hydroxyproline imino acid, which is an important structural moiety responsible for stabilizing the triple helical structure of collagen protein.³⁴ In the study, the total soluble collagen was determined at 7 and 14 day, using Biocolor Sircol collagen assay kit, following the manufacturers' protocol. In brief, the growth medium from the last 3-4 days of the stipulated culture was collected. The secreted total soluble collagen was isolated with 200 μL

of collagen concentrating agent and stored overnight at 4 °C. 500 µL of Sircol dye reagent was added to the colorless total soluble collagen residue, isolated by centrifugation at 12,000 rpm, 4 °C for 10 min. The extracted collagen and dye mixture together were incubated at 37 °C for 30 min. The collagen-dye precipitate that ensued was washed with 750 µL of an ice-cold acid-salt wash reagent to remove the excess dye. Finally, the collagen bound dye was released by the addition of an alkali reagent and the absorbance was read at 555 nm in a plate reader (Tecan).

2.3.5.4 RNA isolation and semi-quantitative polymerase chain reaction (PCR)

In order to isolate the role of substrate magnetization under external field towards osteogenesis, semi-quantitative PCR was carried out for the cells cultured on HA, HA10Fe and HA40Fe samples, treated periodically with 100 mT magnetic field. Runx2, ALP and Col IA were the early osteogenic markers evaluated on day 7 and 14. The expression of the late osteogenic markers (OCN and OPN) was determined on day 14 and 21. The expression of all the genes was normalized w.r.t GAPDH. RNA isolation from the control cells and SMF treated cells on HA-xFe₃O₄ (x = 0, 10 and 40 wt. %) composites was carried out using Ribozol RNA extraction reagent (Amresco), according to the manufacturer's protocol. First strand cDNA was synthesized by reverse-transcription of the extracted RNA using cDNA synthesis kit (Fermentas ThermoScientific). The sense and antisense primer sequences (5'-3') used for the semi-quantitative PCR reactions are listed in **Table 1**. The PCR reaction conditions included an initial denaturation step at 94 °C for 1 min and a final extension step of 72 °C for 5 min along with the PCR reaction performed for 35 cycles in the following steps: denaturation at 94 °C for 45 sec, annealing between 51-60 °C for 45 sec and extension at 72 °C for 1 min. The amplified PCR products were analyzed with the help of 1.2% agarose gel electrophoresis and ethidium bromide staining. The run gels were visualized under gel-doc to obtain the images, which were quantitatively analyzed with NIH ImageJ software and normalized to their respective GAPDH values.

2.3.5.5 Osteocalcin – ELISA

Enzyme-linked immunosorbent assay (ELISA) is a reliable method of detection and quantification of proteins/ antigens present in media/sera. The protein expression of human osteocalcin, a major non-collagenous protein of bone matrix, was quantified by direct ELISA. After 21 days of hMSC culture, the osteocalcin levels were measured with the help of

Osteocalcin human ELISA kit (Invitrogen, KAQ1381), following the instructions given in the manufacturer's protocol. In brief, the media from the 21 day culture was spun down at 3,000 rpm for 5 min to settle the debris and 100 μ L of the control and sample media were added to each well of the ELISA strips. 100 μ L of anti-OST-HRP conjugate was added to each well and incubated for 2 h at RT. Then, the contents of the wells were aspirated and washed thrice with the wash buffer provided in the kit. Subsequently, 100 μ L of stabilized chromogen was added and incubated for 30 min at RT. Finally, the reaction was stopped by immediately adding 100 μ L of stop solution and read at 450nm with a plate reader (Eppendorf AF2200).

2.3.5.6 Matrix mineralization

The matrix mineralization of hMSCs was detected by alizarin red staining after 28 days of culture. The protocol used during staining with alizarin red is briefly mentioned below. For the estimation of the extent of calcium deposition, the cells were fixed in 4% PFA for 30 min and washed thoroughly with deionized (DI) water. The samples were stained with 2% Alizarin Red (Sigma) Solution (ARS, pH ~ 4.1-4.3), incubated in dark at room temperature for 45 min and washed repeatedly (5-6 times) with DI water until there was no residual dye. The observation of the stained samples was performed using the Nikon microscope in the optical bright field mode. For quantification of matrix mineralization, the calcium-alizarin red complex was eluted by incubation with 20% methanol/10% acetic acid for 15 min. The absorbance of 100 μ L of the aliquots was read at 450 nm with a multimode plate reader (Eppendorf AF2200). The background staining for each of the samples was subtracted for quantifying the calcium content. In order to directly observe the mineralized nodules, the substrates after 28 day culture were washed with PBS, fixed with 3.0% (v/v) glutaraldehyde (LobaChemie) in PBS for 20 min at room temperature. The samples were dehydrated by washing with a gradient series of ethanol (30, 50, 70, 90 and 100% v/v), sputter coated with gold and imaged under a Scanning electron microscope (SEM; Inspect F50, FEI, USA) equipped with Energy dispersive x-ray spectrometer (EDX).

2.4 Statistical analysis

The statistical analysis was carried out using IBM SPSS Statistics 20 software. All the experiments were carried out in triplicate and the analysis of variance (one way ANOVA) was adopted to determine the statistical significance between cell response on HA-xFe₃O₄ composites

without and with magnetic field treatment, as compared to the control. For all the data plots, Tukey and Games-Howell tests were employed to determine the statistical significance at $p < 0.05$, where p denotes the probability that there is no significant difference between the means.

3. Results

3.1 Magnetic substrate characterization

The density of the hot pressed HA- $x\text{Fe}_3\text{O}_4$ composites were measured by Archimedes method. Considering the density of HA and Fe_3O_4 are 3.156 and 4.9 g/cc respectively, all the hot-pressed composites were ~95-97% of their theoretical densities (ρ_{th}). The measured density of the samples has been tabulated as percentage of theoretical densities ($\% \rho_{\text{th}}$) in **Table 2** along with the surface wettability data. The contact angle data of the hot-pressed HA- $x\text{Fe}_3\text{O}_4$ composites along with representative images have also been listed in **Table 2**. A linear increase in the surface hydrophobicity or a systematic decrease in the surface wettability with Fe_3O_4 addition can be observed. The increase in the hydrophobic character of the surface is expected to be due to the obvious decrease in the number of polar hydroxyl groups on the surfaces of the composites. Notably, the contact angle data indicate a significant difference in surface wettability of HA40Fe composite as compared to HA and HA5Fe while the surface wettability in HA10Fe and HA20Fe is comparatively distributed over a small range. In summary, the surface hydrophobicity of HA- $x\text{Fe}_3\text{O}_4$ composites increased marginally with Fe_3O_4 addition. The contact angle data reveal that the substrates are hydrophobic in nature and the hydrophobic nature is enhanced at large Fe_3O_4 addition ($x \geq 20$ wt %). Also, relatively dense substrates are used with sinter density of 95-97% ρ_{th} , so that any additional influence of porosity on cell fate processes can be ruled out.

3.1.1 Phase assemblage

X-ray diffraction patterns (**Fig. 2**) of all the composites reveal peak positions corresponding to the two major phases namely hydroxyapatite (HA) and magnetite (Fe_3O_4). A minor third phase of maghemite ($\gamma\text{-Fe}_2\text{O}_3$) was detected only in the HA40Fe composite. The characteristic HA, Fe_3O_4 and $\gamma\text{-Fe}_2\text{O}_3$ were identified with the corresponding standard XRD patterns from the International crystallographic structure database (ICDD: JCPDS card numbers: 84-1998 (HA), 85-1436 (Fe_3O_4) and 24-0081 ($\gamma\text{-Fe}_2\text{O}_3$)). However, reitveld refinement of XRD data gave good fit for wustite (Fe_{1-x}O) as additional minor phase while Fe-doped HA was detected in all the

composites by Mössbauer spectroscopy (data not shown). No major phase transformation of magnetite (Fe_3O_4) to hematite ($\alpha\text{-Fe}_2\text{O}_3$) was detected. Also, no β -tricalcium phosphate ($\beta\text{-TCP}$) by dehydroxylation from HA was observed within the detection limits of XRD.

3.1.2 Microstructure and phase identification

Bright field TEM image (**Fig. 3A**) of HA40Fe composite shows lighter HA grains and darker iron oxide particles, some of which formed aggregates during hot-pressing. Hence, the iron oxide particles ranged from 50-200 nm in size. **Fig. 3B** is the corresponding selected area diffraction pattern from a Fe_3O_4 grain (dark contrast), which was indexed along [001] zone axis. The diffraction pattern is in agreement with the cubic inverse spinel structure of Fe_3O_4 (lattice parameter of 8.393 Å). Such a structure is characterized by O^{2-} anions at the cube corners and face centres of the FCC lattice with all the tetrahedral sites being occupied by Fe^{3+} cations and the octahedral sites equally, by both Fe^{2+} and Fe^{3+} ions. The representative HRTEM images of magnetite (overlapping lattice planes), maghemite ($\gamma\text{-Fe}_2\text{O}_3$) and hydroxyapatite (HA) are shown in **Fig. 3C, D** and **E**, respectively. The corresponding filtered FFTs were indexed for phase identification and have been included as insets in the respective HRTEM images. **Fig. 3F** is a Moire fringe pattern formed by the interference of overlapping crystal planes of HA and Fe_3O_4 . The inset included in **Fig. 3F** is the intensity profile of the Moire fringe pattern which can be deconvoluted to identify the interfering planes. The abundance of Moire patterns in HA40Fe indicates an ordered arrangement/ preferred orientation of the crystallites, which can lead to enhanced ferromagnetic property of the sample. It may be noted that it is difficult to distinguish between magnetite (Fe_3O_4 : Fd3m space group) and maghemite ($\gamma\text{-Fe}_2\text{O}_3$: P4₂32 space group) by XRD and TEM as both of them have cubic inverse spinel structures and nearly identical lattice parameter (8.393 Å and 8.350 Å, respectively).³⁵ However, careful indexing of the FFTs enabled a clear distinction between the two phases. Also, there was no phase transformation of Fe_3O_4 to $\alpha\text{-Fe}_2\text{O}_3$ (rhombohedral symmetry, R $\bar{3}c$ space group with lattice parameters $a = b = c = 5.42$ Å) in the specimens analyzed.

3.1.3 Magnetic properties

The magnetic behavior of HA and Fe_3O_4 are known to be diamagnetic and ferromagnetic, respectively with magnetite nanoparticles (MNPs) having a room temperature saturation magnetization (M_s) of ~75 emu/g. However, in our study, the maximum room temperature

experimental saturation magnetization of pristine Fe_3O_4 NPs with a mean particle size, $d < 50$ nm was measured to be 21.8 emu/g. **Fig.s 4A** and **B** show representative room temperature magnetization curves of HA- $x\text{Fe}_3\text{O}_4$ composites as a function of Fe_3O_4 addition, while **Fig. 4C** corresponds to the magnetic behavior of pure Fe_3O_4 NPs. **Table 3** is a summary of the room temperature magnetic behavior of HA- $x\text{Fe}_3\text{O}_4$ sintered composites along with the assigned magnetic property. It is interesting to note that the saturation magnetization of HA40Fe composite is greater than that of pure Fe_3O_4 NPs, which was used as second phase dispersion in the composites. The Moire patterns observed in the TEM of HA40Fe composite indicate a deliberate orientation of the lattice planes of the two crystals leading to superior ferromagnetic property. Among the sintered composites, it is obvious that the saturation magnetization (M_s), remanant magnetization (M_r) and area under the hysteresis loops of HA- $x\text{Fe}_3\text{O}_4$ composites increase with Fe_3O_4 content. It is also interesting to note that the magnetic field strength required for saturating the magnetization of HA10Fe, HA20Fe and HA40Fe composites are $\sim 1, 2$ and 4 kilogauss respectively, while the magnetization of HA5Fe did not saturate even at 20 kilogauss (data not shown). This is in contrast to bulk Fe_3O_4 , which can be saturated at field $\leq 1\text{kOe}$ for any crystal direction and hence described as magnetically soft.³⁶ The lack of any systematic increase of magnetic property with Fe_3O_4 can be explained by the fact that the rule of mixtures is not applicable with regard to magnetic properties of composites due to the formation of additional paramagnetic phases detected by Mössbauer spectroscopy (unreported data). Additionally, Fe_3O_4 is reported to exhibit magnetic anisotropy with an easy axis of magnetization along the crystallographic [111] direction of the crystal at room temperature. As the particles of Fe_3O_4 in the sintered composites are randomly oriented with respect to the direction of the applied field as against epitaxially grown Fe_3O_4 films, the magnetic properties do not increase proportionately with Fe_3O_4 addition. Among the composites, there was no definite trend for coercive field (H_c), which is another characteristic feature of the magnetic hardness. The relatively coarse grains of Fe_3O_4 in the sintered composites ($\sim 50\text{-}200$ nm, as evident from the bright field TEM image of HA40Fe) as compared to Fe_3O_4 NPs (< 50 nm size), contributes significantly to the ferromagnetic property of the composites as against the weakly superparamagnetic behavior of the Fe_3O_4 NPs.

3.2 Stem cell functionality *in vitro*

In this present study, the effect of substrate magnetization on the osteogenesis of mesenchymal stem cells is being presented. Hence, the magnetic behavior of the composites is being reiterated before the *in vitro* data. Based on the measured magnetic properties, the HA20Fe and HA40Fe composites have been assigned as ferromagnetic and strongly ferromagnetic, respectively while the HA10Fe has been designated as weakly ferromagnetic. The HA5Fe composite is completely paramagnetic while monolithic HA is diamagnetic in nature. The influence of static magnetic field (SMF) exposure on the proliferation and differentiation of hMSCs cultured on these magneto-responsive substrates will be elucidated in the next section.

3.2.1 Magnetic field mildly diminished the viability & proliferation of hMSCs on diamagnetic and paramagnetic substrates, but enhanced progressively from weak to strongly ferromagnetic substrates

Viability: The metabolic activity of hMSCs on HA-xFe₃O₄ composites, cultured with regular intermittent SMF stimulation (as shown in **Fig. 1B**) was determined by MTT assay. **Fig. 5A** is a bar chart of hMSC viability cultured on HA-xFe₃O₄ substrates for 3, 5 and 7 days without and with SMF exposure. The viability of SMF treated hMSCs on diamagnetic HA showed a significant ($p < 0.05$) drop by ~35% and 50% on day 3 and day 5 respectively, followed by a mild recovery at day 7. Among the composites, the cells cultured on HA5Fe (paramagnetic) exhibited a similar behavior under SMF exposure, but with a lesser decrease in viability by ~30% and 25% on day 3 and day 5 respectively, with a similar recovery as HA. In contrast, the weak and strongly ferromagnetic (HA-xFe₃O₄; $x \geq 10$ wt %) substrates facilitated good viability of hMSCs with occasional drops in viability under normal and magnetic field stimulated culture.

Cytotoxicity: The cytotoxicity of HA-xFe₃O₄ composites on hMSCs, cultured without and with SMF exposure was estimated by LIVE/DEAD assay. **Fig. 5C** shows representative images of cells stained with FDA/PI dye combination. The green fluorescence arises from the esterase activity of live cells leading to the deesterification of fluorescein diacetate (FDA) to fluorescein, while the red nuclei represent the dead cells due to the intercalation of propidium iodide (PI) with the DNA of membrane compromised cells. A higher fraction of PI stained cells were observed on HA (diamagnetic) and HA5Fe (paramagnetic) composites in the presence of magnetic field, while the cell density of hMSCs was significantly lower on monolithic HA.

Moreover, the cell morphology of SMF treated hMSCs, cultured on the HA10Fe and HA40Fe ferromagnetic composites appear rhomboidal as against the smaller and spindle-shaped cells seen on substrates with lesser magnetization.

Proliferation: The proliferation of hMSCs was quantitatively determined in terms of the DNA content for each sample. **Fig. 5B** is a bar chart depicting the temporal changes in the proliferation of hMSCs cultured on the magnetic substrates under normal and SMF treated culture. On day 3, the DNA content on all the samples was similar to that of the control except for a moderate decline in HA5Fe paramagnetic composite. A similar drop in the DNA content can be observed on HA and HA5Fe substrates under SMF culture on day 5, finally ending in a delicate recovery on day 7. Among the weak and strongly ferromagnetic composites, the hMSC proliferation ceased, as indicated by the saturation in DNA content after day 5. Thus, SMF stimulation appeared to trigger the differentiation of hMSCs on ferromagnetic substrates.

3.2.2 SMF exposure induces proliferation arrest and increases intracellular calcium levels – cellular events driving the hMSC differentiation.

Cell cycle analysis: The decrease in the proliferation of SMF exposed hMSCs was further detected by flow cytometry based analysis of cell populations distributed in different stages of cell cycle. The acquired data were analyzed with Modfit software. **Fig. 6A** shows representative histogram plots deconvoluted to determine the percentage of cells in the G0/G1 (interphase), S (synthesis) and G2/M (mitotic) phases of the cell cycle. The auto debris and aggregates (false positives) exclusion functions were applied, while fitting the data. The y-axis zoomed plots showing the fit are also shown in **Fig. 6A** for each sample. A significant decrease in the percentage of cells in S phase and an increase of cell populations in G0/G1 phase can be observed in SMF exposed hMSCs cultured on HA10Fe and HA40Fe. **Fig. 6B** shows that around 10% and 5% of cells are in S and G2/M phases, respectively in control, while SMF exposure reduced the S and G2/M phase population to 3% and 2.5% respectively, on the weak and strongly ferromagnetic composites. The reduction in the proportion of cells in the proliferation (S) phase and dividing (G2/M) phase with a concomitant increase in the interphase (G0/G1) population is significant in the HA10Fe and HA40Fe compositions as compared to control and HA. This indicates SMF induced proliferation arrest of hMSCs cultured on the weak and strongly ferromagnetic substrates.

Intracellular calcium levels: As cellular calcium is known to act as a secondary messenger in governing cell fate, flow cytometry was employed to estimate the increase in intracellular calcium (Ca_i) compared to control. **Fig. 6C** is an overlay of representative histogram plots showing cell count versus fluorescence intensity of Ca_i -Fluo-4 complex. A clear increase in the mean fluorescence intensity (MFI) of Ca bound dye can be observed in the SMF treated cells on HA10Fe and HA40Fe samples as compared to the unstimulated control. A 2-2.7 fold increase in the MFI of the SMF exposed hMSCs to that of the control was recorded (**Fig. 6D**). In SMF exposed HA too, the cells exhibited a higher Ca_i level. This anomalous increase can arise as a result of extracellular calcium (pure HA) driven rise in Ca_i , as reported earlier.³⁷ It may also be noted that the observed rise in calcium did not occur as a result of cell apoptosis, wherein high Ca_i is implicated. This is because, the live cell populations were gated identically for the different samples and histograms were constructed over the gated events during data analysis. Further, the samples dual stained with Fluo-4 AM and PI were also analyzed by flow cytometry. The percentages of Fluo-4 stained live cell populations were similar between samples while that of the double-stained ones were not significantly different (data not shown). Thus, the increase in Ca_i due to cell apoptosis can be ruled out. Such a dramatic elevation in Ca_i level, as an immediate response to SMF exposure can trigger downstream signaling pathways that promotes osteogenic gene expression.

3.2.3 A high concentration of extracellular collagen secretion was detected in magnetic field exposed weakly ferromagnetic substrate

The secretion of collagen into the extracellular matrix is a pre-requisite for the formation and homeostasis of bone tissue.³⁸ In the present work, the total soluble collagen was determined by the Sircol collagen assay. The extracellular collagen secreted by hMSCs cultured for 7 and 14 days on magnetic substrates, with simultaneous magnetic field exposure of 100 mT is shown in **Fig. 7**. On day 7, the collagen protein expression attained a maximum in the SMF treated HA10Fe and HA20Fe ferromagnetic composites. The secreted collagen continued to increase significantly ($p < 0.05$) in the SMF treated HA10Fe substrate on day 14. At 2 weeks, all the compositions showed significantly higher collagen secretion, with a maximum of 2-fold increase in the HA20Fe composition, while regular magnetic exposure led to a 3-fold change in the case of HA10Fe. Particularly, hMSCs cultured on substrates under SMF treatment showed a mild

increase in the collagen secretion, compared to its untreated counterparts. In case of the HA40Fe ferromagnetic composite, the observed collagen levels were even lower than diamagnetic HA along with a detrimental secretion pattern under magnetic stimulation. A moderate saturation of collagen secretion was observed for most of the diamagnetic and ferromagnetic substrates at day 7 while continued collagen secretion until day 14 was observed in the HA10Fe weakly ferromagnetic composite.

3.2.4 Effect of brief magnetic stimuli and substrate magnetization on the mRNA expression pattern and protein levels of early differentiation markers

Runx2 immunocytochemistry: In order to verify the progression of hMSCs towards osteogenic commitment, the cells grown on HA-xFe₃O₄ substrates under magnetically stimulated culture conditions for 5 days were stained with Anti-runx2 antibody. Runx2 is a transcriptional factor involved in early osteoblast differentiation. **Fig. 8A** provides fluorescence images showing Runx2 expression in the untreated and the SMF treated samples. Runx2 protein is an intranuclear protein, which is labeled as green in **Fig. 8A**. This preosteoblast transcription factor was nearly absent in the case of control, while similar Runx2 levels were observed for all the samples, without and with SMF exposure. Also, certain morphological signatures of osteoblast-like cells could be observed on the weak and strongly ferromagnetic substrates, exhibiting well spreaded and rhomboidal geometry.

ALP activity: Alkaline phosphatase (ALP) is a metalloenzyme that plays a major role in skeletal mineralization via the enzymatic degradation of pyrophosphate into inorganic phosphate.³⁹ The ALP activity of hMSCs cultured on magnetic HA-xFe₃O₄ composites under normal and regular SMF treated conditions is depicted in **Fig. 8B**. On day 7, ALP activity was higher on paramagnetic and ferromagnetic substrates as compared to the control. However, on day 14, the ALP secretion was significantly ($p < 0.05$) greater for SMF exposed cells grown on weakly ferromagnetic HA10Fe as compared to control and HA. Interestingly, strongly ferromagnetic HA40Fe substrates also displayed comparable ALP activity to HA10Fe_MF even without the application of SMF. On the whole, the ALP activity of hMSCs increased with substrate magnetization, from 1.5 to 6-fold when advancing from paramagnetic HA5Fe to ferromagnetic HA40Fe. Notably, 14 days of SMF exposure caused a maximum of 7-fold increase in ALP activity in weakly ferromagnetic HA10Fe composition.

Early osteogenic markers: Runx2/Cbfa1, ALP and Col IA were chosen as markers for determining the early osteogenesis of hMSCs after SMF stimulation. The fold change in mRNA expression of the above markers was normalized to the house-keeping gene, GAPDH. **Fig. 8C** and **D** show the PCR bands and fold change in mRNA expression of the early marker genes for magnetically stimulated hMSCs cultured on HA-xFe₃O₄ (x = 0, 10 and 40 wt%) composites. Runx2 expression was significantly greater by around two times as compared to the control for all the samples on day 14. No significant difference ($p < 0.05$) in Runx2 expression was observed on day 7 between the samples. Similarly, the expression of ALP was higher on HA and a near two-fold increase was observed in the weakly ferromagnetic HA10Fe composite on day 7. However, ALP expression was 2.5 and 3-fold to that of the control in HA and HA40Fe composite respectively, while it was more than double of control in the HA10Fe composite. Notwithstanding, the expression of Type I collagen (Col IA) exhibited a similar pattern on day 7 and day 14 among the samples. A striking 2-fold increase in Col IA was observed in HA on day 14, while the others presented marginal upregulation as compared to day 7. In summary, the expression of the early osteogenic markers in the weak and strongly ferromagnetic compositions under SMF culture was greater than control, but was similar to diamagnetic HA.

3.2.5 Magnetic field stimulation effectively promoted the expression of late markers of developing preosteoblasts, as well as osteocalcin secretion

Osteocalcin quantification: The amount of osteocalcin (OCN) secreted by the differentiating hMSCs was quantified by direct ELISA after 21 days of culture. **Fig. 9A** presents a histogram plot of osteocalcin (normalized to total protein content) secreted by non-stimulated and SMF treated hMSCs cultured for 21 days on all the composites. Similar levels of osteocalcin were detected for cells cultured on all the composites which were greater than control, but comparable to HA. However, SMF exposure nearly doubled the production of OCN in the weakly ferromagnetic and strongly ferromagnetic substrates (HA10Fe, HA20Fe and HA40Fe), which was significantly ($p < 0.05$) more than control and HA. Thus, SMF appeared to promote OCN production to a greater extent in compositions with higher substrate magnetization.

Late osteogenic markers: BGLAP (human osteocalcin OCN gene) and OPN (osteopontin) were the late differentiation markers used to assess the osteogenic expression of the developing preosteoblasts. **Fig. 9B** and **C** show the PCR bands and fold change in mRNA expression of

OCN and OPN for SMF stimulated hMSCs cultured on HA, HA10Fe and HA40Fe composites. The highest expression of OCN was recorded in weakly ferromagnetic HA10Fe substrate on day 14. However, upon progressive stimulation till day 21, OCN expression was highly upregulated on both the weak and strongly ferromagnetic composites. With regard to OPN expression, a striking feature is the near absence of bands for the control and HA at both the time points. Despite a slight variation in OPN expression between HA10Fe and HA40Fe at the two time points, both of them displayed pronounced upregulation compared to diamagnetic HA. It can be concluded from the gene expression data of late osteogenic markers (OCN and OPN), that SMF stimulation effectively promoted osteogenesis in weak and strongly ferromagnetic substrates to an almost similar extent.

3.2.6 Matrix mineralization and calcium content is greatly increased with increase in substrate magnetization

Alizarin: The extracellular calcium content of the osteogenically differentiating hMSCs was determined after 28 days in culture. **Fig. 10A** shows representative images of Alizarin Red S (ARS) stained hMSCs grown without and with SMF exposure. The hMSCs on control glass cover slip did not show any trace of alizarin red stain, while HA and composites with Fe₃O₄ showed cells stained with alizarin. The calcium content was semi-quantified by measuring the absorbance of the alizarin red extracts. **Fig. 10B** is a histogram plot depicting calcium levels after 28 days of normal and SMF culture. As expected, the maximum absorbance was recorded for the weakly ferromagnetic HA10Fe composition without and with SMF exposure. Likewise, HA40Fe also showed significantly ($p < 0.05$) greater calcium deposition than HA following magnetic stimulation.

SEM-EDX: Matrix mineralization potential of lineage committed hMSCs was observed by imaging under SEM (FEI Inspect) equipped with EDX. Representative images in **Fig. 10C** show nodules of calcium phosphate formed in the HA10Fe and HA40Fe composites with magnetic stimulation. It was observed that the CaP nodules are much smaller in size and uniformly distributed in the ferromagnetic HA40Fe composite while the weakly ferromagnetic HA10Fe composite presented larger and clustered nodules. However, the Ca/P ratio varied from 1.2 to 1.4 with increasing substrate magnetization (HA10Fe to HA40Fe). The Ca/P ratios of the mineral deposits vary with the maturation of bone minerals with time.

4. Discussion

It is known that physical cues (substrate properties, external stimulation) play critical roles in driving a series of stem cell fate processes such as adhesion, proliferation and differentiation.⁴⁰ In the context of bone tissue engineering, it is of extreme importance for the material to possess the potential to actively induce cell differentiation, followed by the expression of osteoblast phenotype in a highly controlled manner.⁴¹ It is also well established that osteogenesis can be modulated by material properties such as porosity, surface roughness (nano versus microscale), stiffness similar to that of bone tissue, surface charge (negatively charged phosphate groups promote mineralization) and surface hydrophilicity/ hydrophobicity (influence protein adsorption and/or may lead to preferential adsorption of osteoinductive proteins). In the current study, sample porosity, roughness, protein adsorption kinetics (**Fig. S1**) and surface wettability were nearly similar, while substrate magnetization was varied among the HA- $x\text{Fe}_3\text{O}_4$ composites. On the other hand, despite numerous investigations on pulsed electromagnetic fields, till date there is no sufficient research in understanding the effect of external magnetic stimuli in promoting osteogenesis of hMSCs. In a quest to predict how stem cells respond differently to static magnetic field depending on the degree of substrate magnetization, three types of HA-based ceramic substrates, were designed. The addition of magnetic phase was tailored so as to specifically obtain a range of magneto-responsive substrates, from dia-, para-, weakly to strongly ferromagnetic matrices (**Table 1**). We observed a smooth variation of magnetization (**Fig. 4**), indicating that the magnetic properties can be readily controlled by tuning the chemical compositions. Such finely tailored material systems with varying degree of magnetization along with magnetic stimuli (protocol shown in **Fig. 1B**) were used to conduct the analysis of substrate magnetization dependent induction of osteogenic activity in hMSCs *in vitro*.

Human mesenchymal stem cells in culture can retain multipotency and can proliferate rapidly when seeded at low densities. However the application of magnetic stimuli to the cells adhered on magnetic substrates, can alter their growth rate. Hence, we verified the proliferation and viability of hMSCs on magnetoactive substrates, by adopting several direct methods such as MTT, PicoGreen and LIVE/DEAD viability/ cytotoxicity assay. At regular time intervals, the growth kinetics of hMSCs cultured on substrates with higher degree of magnetization (weak to strongly ferromagnetic), differed from the less magnetic substrates (dia/paramagnetic),

irrespective of magnetic field application. In non-stimulated group, less magnetic substrates (HA, HA5Fe) showed a delayed growth rate as compared to moderate and highly magnetic substrates (HA10Fe, HA20Fe and HA40Fe) that reached confluency well ahead and displayed a plateau phase in 7 day-old-monolayer. These results further demonstrate that hMSCs respond not only faster but also more dramatically to magnetic stimuli on substrates with higher magnetization. Although highest proliferation was marked in ferromagnetic substrates, the cell density at the end of 7 days was similar for weakly (HA10Fe) to strongly ferromagnetic (HA40Fe) substrates, even in the presence of magnetic stimuli. A plausible explanation for the drop in proliferation in dia/para-magnetic substrate is that the magnetic field lines penetrate into samples with greater ferromagnetic property and the associated magnetic force or energy is dissipated through the alignment of magnetic dipoles along the field. Thus, the ferromagnetic substrates screen the cells from direct field exposure and act as sinks to drain the excess magnetic field. Together, our findings suggest that magnetic substrates critically enhance the viability and DNA synthesis of hMSCs, given that these substrates along with magnetic stimuli can be considered for their potential to promote tissue regeneration to combat bone loss.

After identifying the higher proliferative capacity of hMSCs on weakly and strongly ferromagnetic substrates, our second goal was to examine its role in regulating osteogenic differentiation. hMSCs are known to have the intrinsic ability to differentiate into multiple cell lineages, such as osteoblasts, adipocytes, chondrocytes, etc. To induce *in vitro* osteogenesis of MSCs, a combination of different biochemical induction factors have been suggested in the literature. Instead of basal medium supplementation with induction factors, some studies have even documented the involvement of physical factors such as mechanical stress, pulsed electromagnetic field and hydrostatic pressure in stimulating osteogenic differentiation of progenitor cells.⁴² In this context, we explored the role of substrate magnetization in magnetic field stimulated culture conditions, to understand how they direct osteogenic differentiation of hMSCs. Physiologically, the process of new bone formation is initiated by the differentiation of mesenchymal progenitor cells into osteoblasts⁴³ and the induction of extracellular matrix formation is considered as one of the hallmark for osteogenic differentiation.⁴⁴ Collagen, being the major structural and functional component of ECM, provides foundation for mineral deposition by initiating calcium nucleation sites and calcium phosphate synthesis.^{45, 46} The specific ECM secretory response of hMSCs in response to varying degree of magnetization, was

unveiled by determining the accumulation of total collagen in the cell culture medium. Interestingly, the total collagen synthesis and secretion were accelerated profoundly when cells were cultured in the presence of magnetic stimuli, on weakly ferromagnetic (HA10Fe) substrates (**Fig. 7**). In this respect, such a differentiation-dependent collagen secretion was reported by Uddin *et al.*,⁴⁷ with the application of low intensity pulsed ultrasound. In the present study, the enhanced secretion of collagen in weakly ferromagnetic substrates is believed to facilitate cellular adhesion (**Fig. 5C**) and matrix mineralization (**Fig. 10B**) in the presence of magnetic stimuli.

The commitment and differentiation of MSCs towards osteogenic lineage is tightly regulated by a certain group of factors.⁴⁸ Among those osteogenic factors, the foremost and crucial regulator determining the fate is the osteo-lineage transcription factor, Runx2. After magnetic field treatment on substrates with varying degree of magnetization, we examined the expression level of Runx2 as well as its downstream target genes, including Col IA, OPN and OCN gene. Herein, our data demonstrate an elevated level of Runx2 gene expression in cultures on weakly (HA10Fe) as well as strongly ferromagnetic (HA40Fe) substrates without statistically significant difference, even in the absence of chemical or growth inducers (**Fig. 8D**). Although the Runx2 protein content was detected in all HA-based substrates, the nuclear localization of these factors were more intense on substrates with high degree of magnetization (**Fig. 8A**). We further investigated whether substrate magnetization promotes OCN gene expression in a similar way, as this bone specific marker is Runx2-responsive. Comparatively, a similar fold increase in mRNA expression was noticed on weakly and strongly ferromagnetic substrates (HA10Fe and HA40Fe) depicted in **Fig. 9C**. Overall, these results suggest that ferromagnetic substrates in combination with magnetic stimuli promoted Runx2 and OCN gene expression with respect to diamagnetic substrates. Notably, when analyzing the osteocalcin secreted in the medium after 21 days, we noticed a similar increase in protein level with increasing substrate magnetization i.e. from weak to strongly ferromagnetic substrates (**Fig. 9A**). Among all the osteogenic markers investigated, OPN showed the largest escalation, after 14 days of magnetic stimulation on strongly ferromagnetic substrate (HA40Fe). The same was observed for weakly ferromagnetic (HA10Fe) substrate to a similar extent on day 21, whereas the impact was minimal in control and diamagnetic substrates, with barely detected level of OPN genes. OPN is believed to be an important regulator determining the osteogenic lineage commitment of hMSCs. For instance,

genetic ablation and blockage of OPN accelerated the adipogenic differentiation and retarded the osteogenic differentiation of MSC.⁴⁹ This unambiguously establishes the progression of hMSCs towards osteogenic lineage on SMF exposed ferromagnetic substrates.

Also found at an early stage is the expression of another osteogenic marker, Col IA. Although Col IA expression was high in weakly (HA10Fe) and strongly ferromagnetic (HA40Fe) substrates, the highest level was recorded in diamagnetic material on day 14. The current observation can be correlated to the findings by Lee *et al.* and Nieto *et al.*^{50, 51} suggesting the role of reduced growth rate and intracellular stress effect on Col IA gene expression. Likewise, in our study, as demonstrated in **Fig. 5A**, the slower cell growth and reduced viability in diamagnetic substrates appears to be one of the probable reasons for increased collagen mRNA levels. On the other hand, it is well established that type I collagen enhances the expression of the differentiated phenotype of osteoblasts and accelerates mineralization of the matrix *in vitro*.³⁸ Hence, a considerable rise in collagen mRNA level along with enhanced expression of other osteogenic factors (Runx2, OCN and OPN) in weakly ferromagnetic substrates highlights the directed differentiation of hMSCs towards osteogenic lineage.

Moreover, we found that hMSCs exposed to magnetic stimuli have high mRNA levels of ALP in weakly ferromagnetic substrates on day 7, while the level was almost identical on day 14, irrespective of the substrate magnetization (**Fig. 8D**). Conversely, a striking rise in ALP activity was noticed per cell on weakly ferromagnetic (HA10Fe) substrate, in the presence of magnetic stimuli after 2 weeks. Besides, the non-stimulated hMSCs also elucidated a comparable increase in ALP activity, when cultured on strongly ferromagnetic (HA40Fe) substrate (**Fig. 8B**). Thus, it is illustrious that even strongly ferromagnetic substrates can encourage early stage switch over to osteogenic lineage in the absence of external magnetic stimuli, yet not commensurate with the effect on weakly ferromagnetic substrates under SMF exposure. A slight disparity in the ALP gene and protein expression pattern suggests the regulatory effects of magnetic substrates and magnetic stimuli both at the transcriptional and translational level. Theoretically, it is assumed that there is a correlation between the level of mRNA expressed and that of protein synthesized.⁵² Instead, there may not be a direct correlation because of the multiple steps involving complicated post-transcriptional mechanisms turning mRNA into protein, resulting in erroneous extrapolation of protein concentrations from mRNA levels.⁵³ Protein turnover can vary

significantly depending on a number of different conditions and the cell in turn can control the rates of degradation or synthesis for a given protein.⁵⁴ Likewise, the decreased ALP activity in HA and HA40Fe regardless of higher mRNA level, could be due to diminished rate of synthesis or altered conformation leading to enzyme inactivity.^{52, 55, 56} Having investigated the gene expression profile, we also assessed the matrix mineralization capacity of magnetic field stimulated hMSCs on magnetic platforms, at the final stage on day 28. The results depicted mineralized nodules (**Fig. 10C**) and calcium deposition (**Fig. 10A**) with increase in magnetization and with SMF exposure.

We speculate that the field induced magnetic dipole orientation in ferromagnetic substrates causes localized mechanical stresses, resulting in cellular deformations (**Fig. 11**). It is hypothesized that activation of mechanotransduction pathways through physical stresses stimulate mechano-sensitive calcium channels. Similarly, other downstream signaling pathways including MAPK, β -catenin and Akt and FAK pathway, are also implicated in the osteogenesis of precursor cells.⁵⁷ Knowing the fact that calcium signaling is often sufficient to exert certain cellular behaviour,⁵⁸ we decided to check whether the observed osteogenic lineage commitment in response to SMF exposure is mediated by an increase in Ca_i concentration. To demonstrate its direct contribution, the cytosolic Ca_i level was quantified using flow cytometry, immediately after SMF exposure. As expected, SMF exposure resulted in an elevated intracellular calcium concentration with increasing substrate magnetization (**Fig. 6D**). This substrate magnetization dependent increase in Ca_i level is postulated to be the key regulator transmitting a cascade of cues via cellular signal transduction pathways to the nucleus thereby, inducing the expression of specific genes involved in osteogenic differentiation.⁵⁹ Moreover, we also provide evidence of SMF inducing G0/G1 arrest in hMSCs grown on substrates with increasing magnetization (**Fig. 6B**). Cell cycle arrest at G0/G1 is a critical step at which cells commonly undergo a transition to differentiation.⁶⁰ Although these results suggest that SMF causes shortening of S and G2/M phase, proliferation never seemed to cease completely. Even while undergoing terminal osteogenic differentiation, a certain population of hMSCs still continued to proliferate.^{57, 61}

Apart from monitoring the cellular events that trigger osteogenesis, it may be emphasized that in the present study no additional differentiation factors were used in the MSC media other than the intermittent delivery of magnetic stimuli in 48 h interval. These results indicate that magnetic

stimuli could be used to regulate osteogenic differentiation of MSCs on magnetic substrates, without addition of osteogenic factors, which may have important implications in bone tissue engineering. Moreover, these results provide an important insight into the regulatory effect exerted by the magnetic force induced physical stresses that are capable of producing required cues to drive hMSC differentiation *in vitro*. Finally, we summarize the temporal trend in the expression of specific bone marker genes. As pointed out earlier, the addition of Fe₃O₄ promoted cell proliferation under SMF exposure, which led to earlier confluency of cells on such substrates. Further, SMF exposure of cells on ferromagnetic compositions (HA10Fe and HA40Fe) resulted in proliferation arrest and increased intracellular calcium, Ca_i. The expression of the early osteogenic markers (Runx2, ALP and Col IA) for HA, HA10Fe and Ha40Fe were moderately upregulated on day 7 and progressively elevated on day 14. Notwithstanding, SMF treatment triggered a spike in ALP activity and total soluble collagen for cells cultured on HA10Fe at day 14. The enhanced secretion of collagen matrix laid the foundation for the production of osteocalcin and osteopontin (two non-collagenous proteins) and further mineralization of calcium phosphate. With respect to the late bone development markers analyzed on day 14 and 21, SMF enhanced the gene expressions for osteocalcin and osteopontin by manifold, exclusively for HA10Fe and HA40Fe samples. As ALP and OCN regulate osteoblast mineralization, the calcium deposition quantified by ARS staining on day 28 was in commensurate with previously detected OCN levels by ELISA on day 21. Overall, it may be concluded that substrate magnetic properties and external magnetic fields can be employed to achieve magneto-responsive substrate guided differentiation of hMSCs. Taken together the present work along with our earlier published work,⁴⁰ we establish the combinatorial physical cues (substrate electrical and magnetic properties and corresponding stimulation) in guiding hMSC differentiation through different lineages.

5. Conclusions

The synergistic effect of magneto-responsive substrates and external magnetic field on the osteogenic differentiation of human mesenchymal stem cells is demonstrated in the present study. By the incorporation of varying amounts of Fe₃O₄ into HA matrix, magneto-responsive substrates with increasing magnetization were designed. Our results indicate that weak and strongly ferromagnetic substrates provided a suitable platform for the enhanced osteogenesis of

hMSCs under SMF exposure. In particular, the early osteogenic markers (Runx2, ALP and Col IA) were significantly upregulated compared to control, while the late marker expressions of OCN and OPN along with matrix mineralization were specifically elevated for the weak (HA10Fe) and strongly ferromagnetic (HA40Fe) composites. The flow cytometry analysis indicates that SMF induces proliferation arrest of cells cultured on the ferromagnetic composites leading to their early differentiation. Also, the significant increase of intracellular calcium by SMF potentially guides the hMSCs towards osteogenic lineage. In summary, our work demonstrates that the magnetic field assisted culture of hMSCs on magneto-responsive substrates can be an efficient strategy to manipulate stem cell response and regulate osteogenesis. These findings emphasize the concealed potential of physical stimulation methods as alternatives for stem cell differentiation, without the need of additional growth factors.

Acknowledgements:

This work was supported with funding from the Department of Science and Technology (DST) and the Department of Biotechnology (DBT), Government of India. The authors thank Dr. Girish Kunte, Suma (MNCF, CeNSE, IISc), Prof. N.Ravishankar (MRC, IISc) and AFMM facility for helping with TEM sample preparation and microscopy. Also, the authors are grateful to Dr. Rajeev Ranjan (Materials Engineering) and Venkatesh (Ph.D. student) for helping with VSM measurements. One of the authors, Sunil Kumar B (09/079 (2501)/2011-EMR-I dt. 16-11-2011) acknowledges the Council for Scientific and Industrial Research (CSIR) for providing scholarship during the period of study.

Supporting Information:

The supporting information pertains to the kinetics of serum protein adsorption of HA-Fe₃O₄ composites. It contains the protocol and results as a supplementary figure (**Fig. S1**). This information is made available from the online library or the author.

List of tables:

Table 1: Primer sequences and PCR reaction conditions

Gene	Forward and reverse primer sequences (5'-3')	Annealing temperature (°C)	Product size (bp)	Annotation ID
GAPDH (house keeping)	AGGTCGGTGTGAACGGATTTG TG TAGACCATGTAGTTGAGGTCA	55	123	NM_002046.5
Runx2	ATGGCGGGTAACGATGAAAAT ACGGCGGGGAAGACTGTGC	58	421	NM_004348.3
Col IA	TACCCCACTCAGCCCAGTGT ACCAGACATGCCTCTTGTCCTT	60	76	NM_000088.3
ALPL	TGGAGCTTCAGAAGCTCAACACCA ATCTCGTTGTCTGAGTACCAGTCC	51	454	NM_000478.4
BGLAP (OCN)	ATGAGAGCCCTCACACTCCTC GCCGTAGAAGCGCCGATAGGC	60	294	NM_199173.4
SPP1(OPN)	CCTCCTAGGCATCACCTGTG CCACACTATCACCTCGGCC	58	422	NM_000582.2

Table 2: Density and surface hydrophilicity/ hydrophobicity of HA- xFe₃O₄ composites determined by Archimedes and contact angle measurement using sessile water drop method, respectively

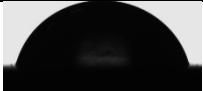

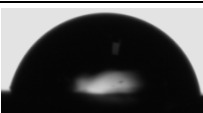
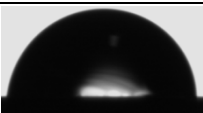
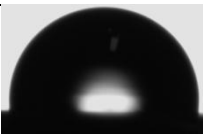
Sample	% theoretical density (ρ_{th})	Contact angle (°)	Image of the water droplet
HA	96.2 ± 1.4	76.3 ± 2.9	
HA5Fe	94.7 ± 1.5	75.6 ± 1.4	
HA10Fe	95.4 ± 1.2	78.1 ± 1.6	
HA20Fe	95.4 ± 1.5	83.2 ± 2.9	
HA40Fe	96.8 ± 1.7	98.9 ± 4.9	

Table 3: Room temperature magnetic properties of HA-xFe₃O₄ composites as recorded by VSM

Sample	Remanance magnetization M _r (emu/g)	Saturation magnetization M _s (emu/g)	Coercive field H _c (G)	Area within M-H loop (G*emu/g)	Assigned magnetic property
HA40Fe	4.31 ± 1.1	25.51 ± 5.9	147.2 ± 22.7	(1.8 ± 0.5)* 10 ⁶	Strongly ferromagnetic
HA20Fe	1.25 ± 0.8	5.95 ± 2.2	178.2 ± 52.8	(3.7 ± 1.9)* 10 ⁵	Ferromagnetic
HA10Fe	0.32 ± 0.2	1.79 ± 1.1	160.2 ± 30.6	(7.8 ± 4.2)* 10 ⁴	Weakly ferromagnetic
HA5Fe	(7.5 ± 2.3)*10 ⁻⁴	ND	104.1 ± 42.4	(3.9 ± 2.3)* 10 ³	Paramagnetic
Fe ₃ O ₄ NPs	2.30 ± 0.9	17.30 ± 5.2	88.4 ± 10.5	(7.6 ± 2.3)*10 ⁵	Weakly superparamagnetic /ferromagnetic

ND – not detected

References:

1. S. D. Subramony, B. R. Dargis, M. Castillo, E. U. Azeloglu, M. S. Tracey, A. Su and H. H. Lu, *Biomaterials*, 2013, **34**, 1942-1953.
2. A. K. Dubey, S. D. Gupta and B. Basu, *J Biomed Mater Res B Appl Biomater.* , 2011, **98**, 18-29.
3. H. Kaji, M. Nishizawa and T. Matsue, *Lab Chip.* , 2003, **3**, 208-211.
4. C. L. Bassett, S. N. Mitchell and S. R. Gaston, *JAMA*, 1982, **247**, 623-628.
5. C. A. Bassett and M. Schink-Ascani, *Calcified Tissue International*, 1991, **49**, 216-220.
6. G. Borsalino, M. Bagnacani, E. Bettati, F. Fornaciari, R. Rocchi, S. Uluhogian, G. Ceccherelli, R. Cadossi and G. C. Traina, *Clin Orthop Relat Res.* , 1988, **237**, 256-263.
7. G. I. Mammi, R. Rocchi, R. Cadossi, L. Massari and G. C. Traina, *Clin Orthop Relat Res.* , 1993, **288**, 246--253.
8. R. J. Midura, M. O. Ibiwoye, K. A. Powell, Y. Sakai, T. Doehring, M. D. Grabiner, T. E. Patterson, M. Zborowski and A. Wolfman, *J Orthop Res.* , 2005, **23**, 1035-1046.
9. C. T. Rubin, K. J. McLeod and L. E. Lanyon, *J Bone Joint Surg Am.* , 1989, **71**, 411-417.
10. F. Tabrah, M. Hoffmeier, F. Gilbert, Jr., S. Batkin and C. A. Bassett, *J Bone Miner Res.* , 1990, **5**, 437-442.
11. C. H. Lohmann, Z. Schwartz, Y. Liu, H. Guerkov, D. D. Dean, B. Simon and B. D. Boyan, *J Orthop Res.* , 2000, **18**, 637-646.
12. A. Icaro Cornaglia, M. Casasco, F. Riva, A. Farina, L. Fassina, L. Visai and A. Casasco, *Eur J Histochem.* , 2006, **50**, 199-204.
13. H. Zhou and J. Lee, *Acta Biomaterialia*, 2011, **7**, 2769-2781.
14. W. Yang, X. Xi, J. Fang, P. Liu and K. Cai, *Mater Sci Eng C Mater Biol Appl.* , 2013, **33**, 3753-3759.

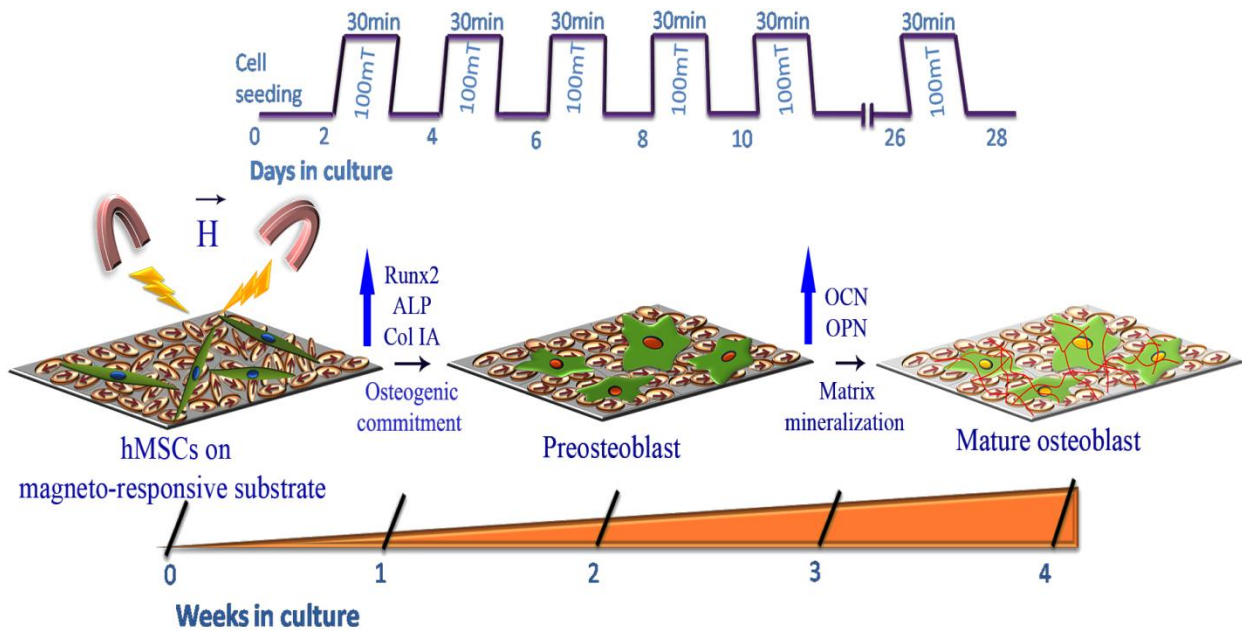
15. M. Ajeesh, B. F. Francis, J. Annie and P. R. Harikrishna Varma, *J Mater Sci Mater Med.* , 2010, **21**, 1427-1434.
16. H. Jiang, Y. Li, Y. Zuo, W. Yang, L. Zhang, J. Li, L. Wang, Q. Zou and L. Cheng, *J Nanosci Nanotechnol.* , 2009, **9**, 6844-6850.
17. A. Kasten, P. Muller, U. Bulnheim, J. Groll, K. Bruellhoff, U. Beck, G. Steinhoff, M. Moller and J. Rychly, *J Cell Biochem.* , 2010, **111**, 1586-1597.
18. J. Dobson, *Nat Nanotechnol.* , 2008, **3**, 139-143.
19. S. H. Song, J. Choi and H. I. Jung, *Electrophoresis.* , 2010, **31**, 2762-2770.
20. N. Tran and T. J. Webster, *Acta Biomater.* , 2010, **7**, 1298-1306.
21. N. Tran, D. Hall and T. J. Webster, *Nanotechnology.* , 2012, **23**, 455104.
22. S. Panseri, C. Cunha, T. D'Alessandro, M. Sandri, G. Giavaresi, M. Marcacci, C. T. Hung and A. Tampieri, *J Nanobiotechnology.* , 2012, **10**.
23. I. Bajpai, K. Balani and B. Basu, *Journal of Biomedical Materials Research Part B: Applied Biomaterials*, 2014, **102**, 524-532.
24. A. K. Dubey, P. Agrawal, R. D. Misra and B. Basu, *J Mater Sci Mater Med.* , 2013, **24**, 1789-1798.
25. A. K. Dubey and B. Basu, *Journal of the American Ceramic Society*, 2014, **97**, 481-489.
26. G. Thirvikraman, P. K. Mallik and B. Basu, *Biomaterials*, 2013, **34**, 7073-7085.
27. S. Jain, A. Sharma and B. Basu, *Biomaterials.* , 2013, **34**, 9252-9263.
28. I. Bajpai, N. Saha and B. Basu, *J Biomed Mater Res B Appl Biomater.*, 2012, **100**, 1206-1217.
29. P. Pozarowski and Z. Darzynkiewicz, *Methods Mol Biol.* , 2004, **281**, 301-311.
30. S. W. Burchiel, B. S. Edwards, F. W. Kuckuck, F. T. Lauer, E. R. Prossnitz, J. T. Ransom and L. A. Sklar, *Methods.* , 2000, **21**, 221-230.
31. M. Zayzafoon, *J Cell Biochem.* , 2006, **97**, 56-70.
32. S. Sun, Y. Liu, S. Lipsky and M. Cho, *FASEB J.* , 2007, **21**, 1472-1480.
33. S. Nath, S. Kalmodia and B. Basu, *J Biomater Appl.* , 2011, **27**, 497-509.
34. R. R. Lareu, D. I. Zeugolis, M. Abu-Rub, A. Pandit and M. Raghunath, *Acta Biomater.* , 2010, **6**, 3146-3151.
35. D. Tripathy, A. O. Adeyeye and S. Shannigrahi, *Physical Review B*, 2007, **76**, 174429.
36. J. E. Lima, A. L. Brandl, A. D. Arelaro and G. F. Goya, *Journal of Applied Physics*, 2006, **99**, 083908-083910.
37. M. M. Dvorak, A. Siddiqua, D. T. Ward, D. H. Carter, S. L. Dallas, E. F. Nemeth and D. Riccardi, *Proceedings of the National Academy of Sciences of the United States of America*, 2004, **101**, 5140-5145.
38. S. Shi, M. Kirk and A. J. Kahn, *J Bone Miner Res.* , 1996, **11**, 1139-1145.
39. E. E. Golub and K. Boesze-Battaglia, *Current Opinion in Orthopaedics*, 2007, **18**, 444-448
40. G. Thirvikraman, G. Madras and B. Basu, *Biomaterials.* , 2014, **35**, 6219-6235.
41. D. S. Benoit, M. P. Schwartz, A. R. Durney and K. S. Anseth, *Nat Mater.* , 2008, **7**, 816-823.
42. E. Birmingham, G. L. Niebur, P. E. McHugh, G. Shaw, F. P. Barry and L. M. McNamara, *Eur Cell Mater.* , 2012, **23**, 13-27.
43. S. M. Zurich, M. Valdovinos, T. Douglas, D. Walterhouse, P. Iannaccone and M. L. Lamm, *Mol Cancer.*, 2012, **11**.

44. C. H. Ku, P. H. Johnson, P. Batten, P. Sarathchandra, R. C. Chambers, P. M. Taylor, M. H. Yacoub and A. H. Chester, *Cardiovasc Res.* , 2006, **71**, 548-556.
45. R. M. Delaine-Smith, S. MacNeil and G. C. Reilly, *Eur Cell Mater.*, 2012, **24**, 162-174.
46. M. R. Khan, N. Donos, V. Salih and P. M. Brett, *Bone.* , 2012, **50**, 1-8.
47. S. M. Uddin and Y. X. Qin, *PLoS One.* , 2013, **8**, e73914.
48. Y. Zhang, D. Khan, J. Delling and E. Tobiasch, *ScientificWorldJournal.* , 2012, **2012**.
49. Q. Chen, P. Shou, L. Zhang, C. Xu, C. Zheng, Y. Han, W. Li, Y. Huang, X. Zhang, C. Shao, A. I. Roberts, A. B. Rabson, G. Ren, Y. Zhang, Y. Wang, D. T. Denhardt and Y. Shi, *STEM CELLS*, 2014, **32**, 327-337.
50. G. H. Lee, H. W. Oh, H. D. Lim, W. Lee, H. J. Chae and H. R. Kim, *Korean J Physiol Pharmacol.*, 2011, **15**, 345-351.
51. N. Nieto, S. L. Friedman, P. Greenwel and A. I. Cederbaum, *Hepatology.* , 1999, **30**, 987-996.
52. D. M. Reffitt, N. Ogston, R. Jugdaohsingh, H. F. Cheung, B. A. Evans, R. P. Thompson, J. J. Powell and G. N. Hampson, *Bone.* , 2003, **32**, 127-135.
53. R. C. Taylor, B. J. Webb Robertson, L. M. Markillie, M. H. Serres, B. E. Linggi, J. T. Aldrich, E. A. Hill, M. F. Romine, M. S. Lipton and H. S. Wiley, *Integr Biol (Camb).* , 2013, **5**, 1393-1406.
54. D. Greenbaum, C. Colangelo, K. Williams and M. Gerstein, *Genome Biol.* , 2003, **4**, 117.
55. J. M. Pratt, J. Petty, I. Riba-Garcia, D. H. Robertson, S. J. Gaskell, S. G. Oliver and R. J. Beynon, *Mol Cell Proteomics.* , 2002, **1**, 579-591.
56. R. Lichtinghagen, P. B. Musholt, M. Lein, A. Romer, B. Rudolph, G. Kristiansen, S. Hauptmann, D. Schnorr, S. A. Loening and K. Jung, *Eur Urol.* , 2002, **42**, 398-406.
57. M. Chiquet, V. Tunc-Civelek and A. Sarasa-Renedo, *Appl Physiol Nutr Metab.* , 2007, **32**, 967-973.
58. G. R. Crabtree, *Cell.* , 1999, **96**, 611-614.
59. A. Liedert, D. Kaspar, R. Blakytyn, L. Claes and A. Ignatius, *Biochem Biophys Res Commun.* , 2006, **349**, 1-5.
60. N. Zhang, M. D. Ying, Y. P. Wu, Z. H. Zhou, Z. M. Ye, H. Li and D. S. Lin, *PLoS One.* , 2014, **9**, e98973.
61. Carlos Vinícius Buarque de Gusmao, Jose Ricardo Lenzi Mariolani and W. D. Belangero, in *Osteogenesis*, ed. P. Y. Lin, InTech, Editon edn., 2012.

The table of contents

Substrate magnetization as a tool for modulating the osteogenesis of human mesenchymal stem cells for bone tissue engineering applications

TOC figure



List of figures:

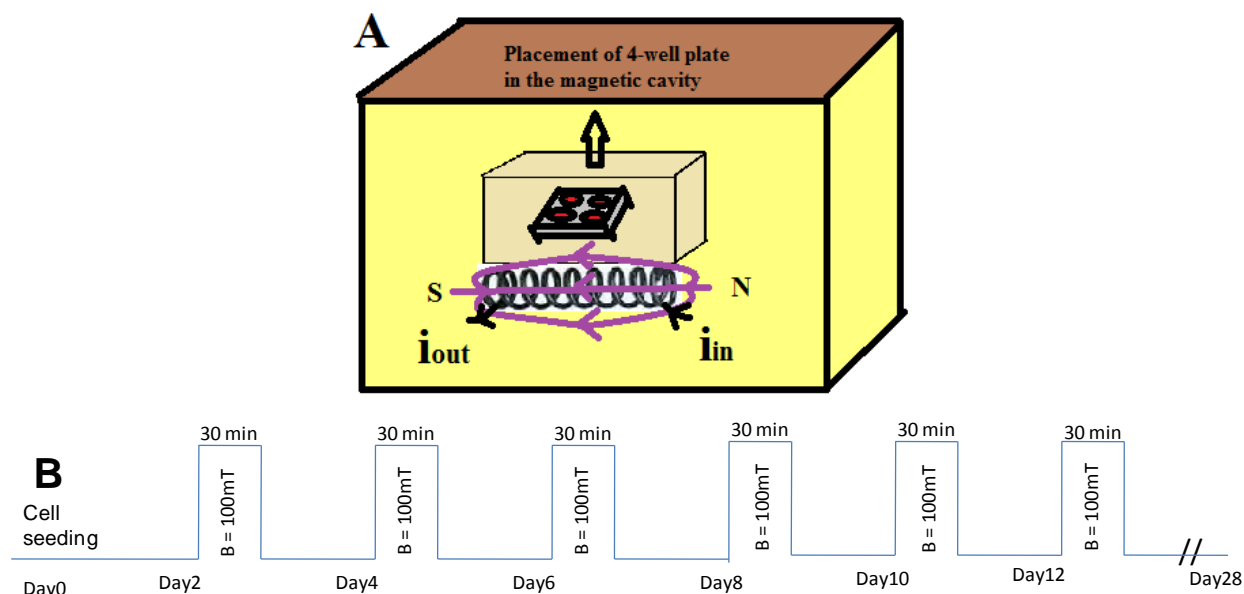


Fig. 1: (A) Schematic of the coil used for generating static magnetic field (100mT) showing the placement of samples in the cavity along with coil current (i) and magnetic field direction; N-North and S-south. (B) Magnetic field exposure cycles used for the treatment of hMSCs seeded on HA- $x\text{Fe}_3\text{O}_4$ composites

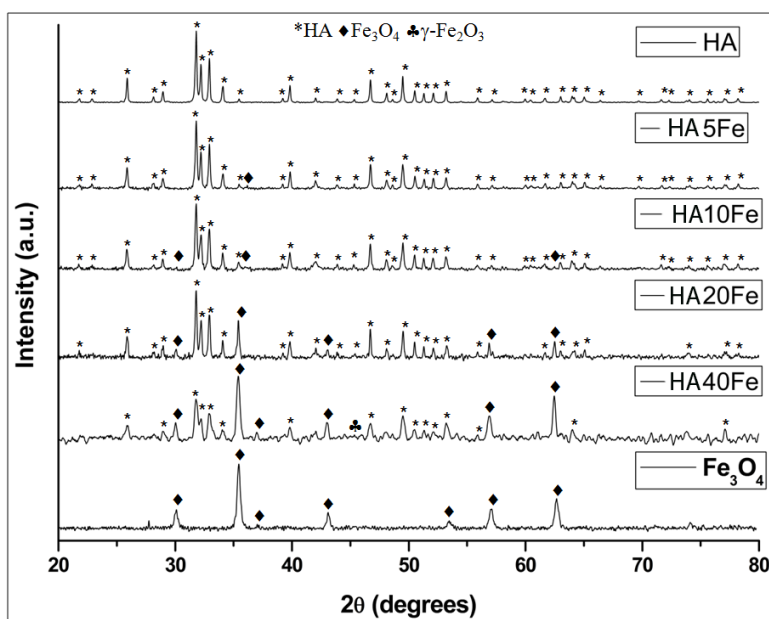


Fig. 2: XRD patterns of hot-pressed HA- $x\text{Fe}_3\text{O}_4$ composites ($x = 5, 10, 20$ and 40 wt% Fe_3O_4) along with calcined HA and pristine Fe_3O_4 NPs ($d < 50$ nm). The characteristic peak positions of the phases present in the hot-pressed samples have been marked by different symbols

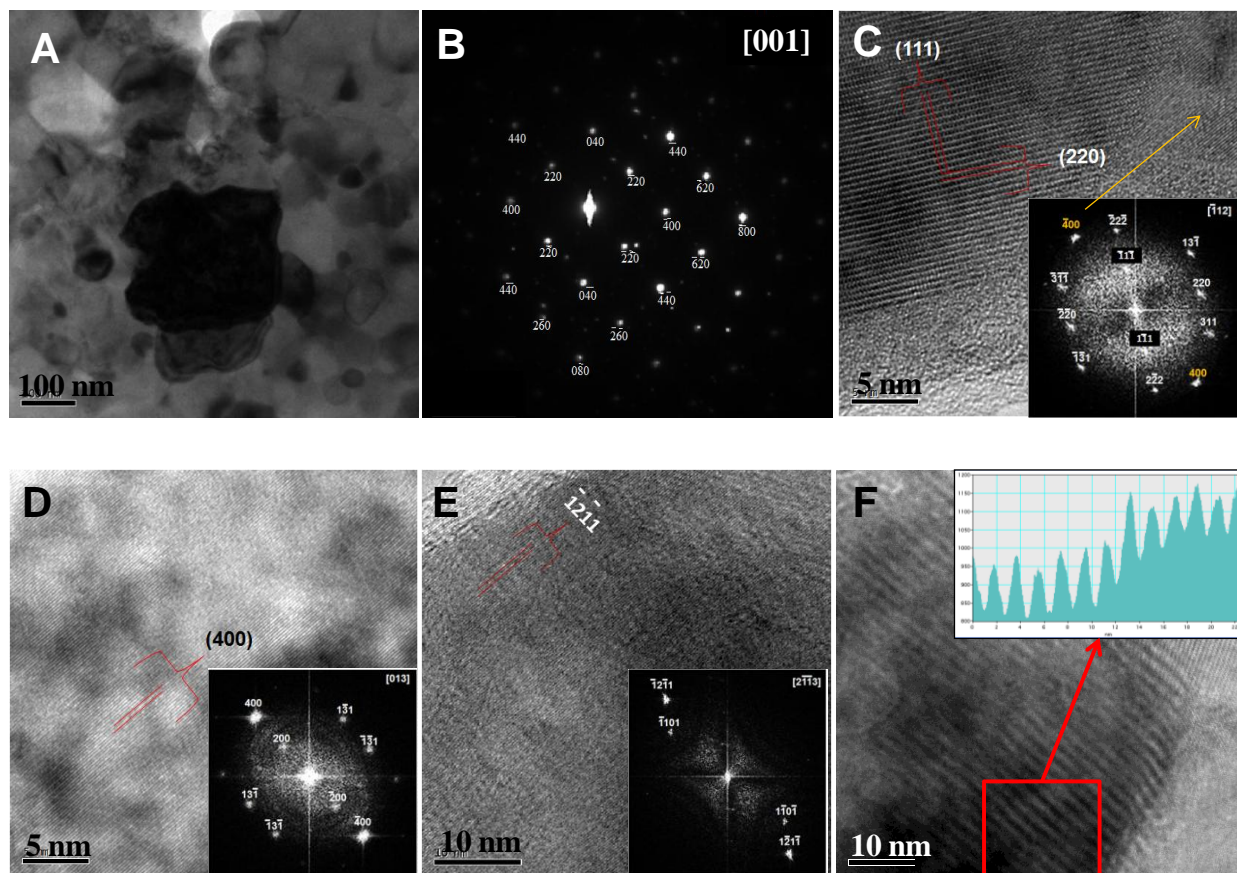


Fig. 3: TEM analysis of sintered HA40Fe (A) Bright field image showing HA and Fe_3O_4 grains, (B) SADP of Fe_3O_4 crystal along [001] zone axis. HRTEM of (C) Fe_3O_4 (D) $\gamma\text{-Fe}_2\text{O}_3$, and (E) HA (corresponding FFTs are included as insets) (F) HRTEM showing Moire fringe pattern formed by overlapping HA and Fe_3O_4 crystal planes (Inset shows the intensity profile in the marked region).

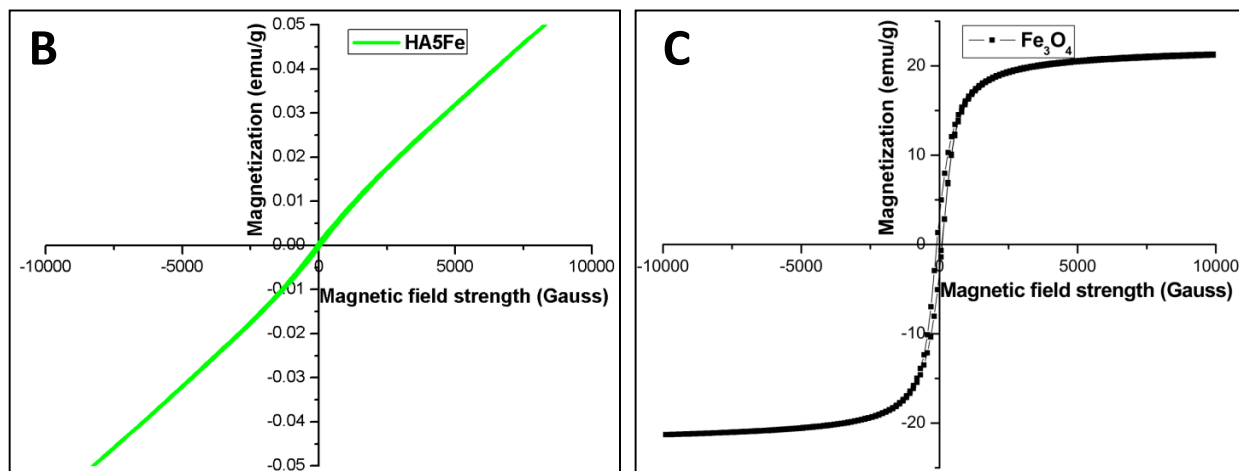
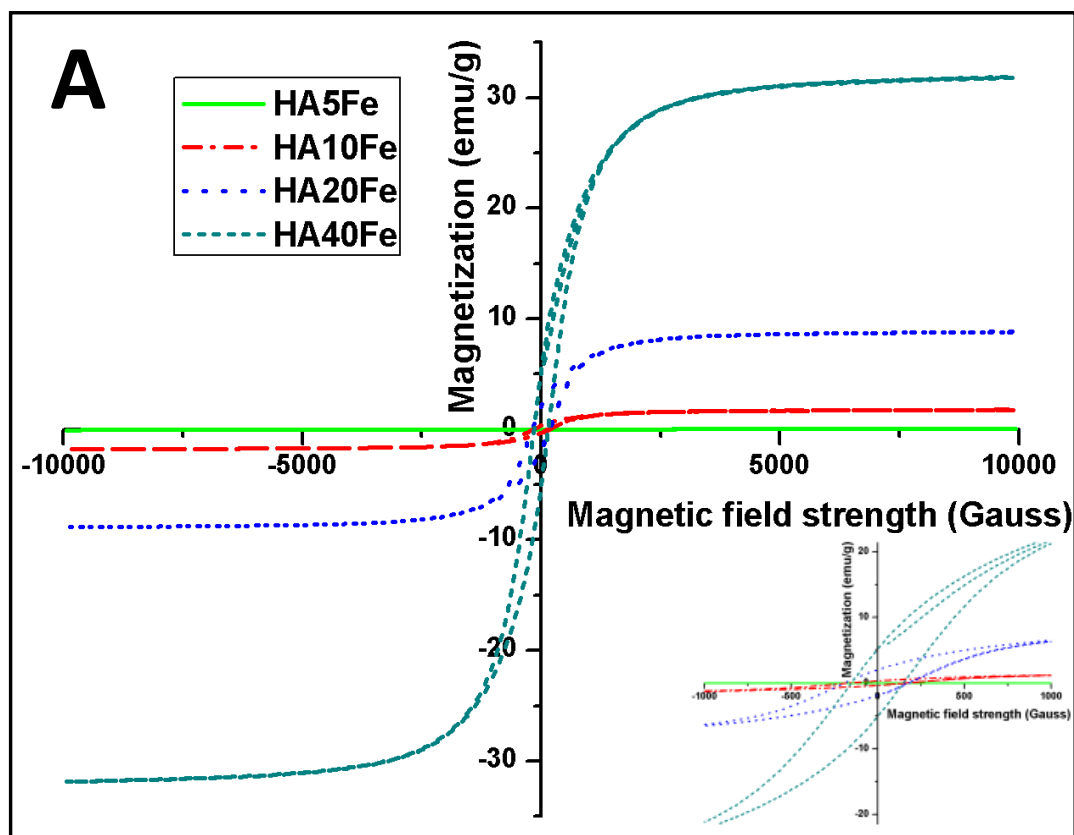


Fig. 4: Room temperature magnetization curves showing M-H curves for (A) HA- x Fe₃O₄ hot-pressed composites with the inset showing clear ferromagnetic hysteresis loops; (B) magnified image of HA5Fe composite exhibiting paramagnetic behavior and (C) M-H curve of pristine Fe₃O₄ NPs with $d < 50$ nm

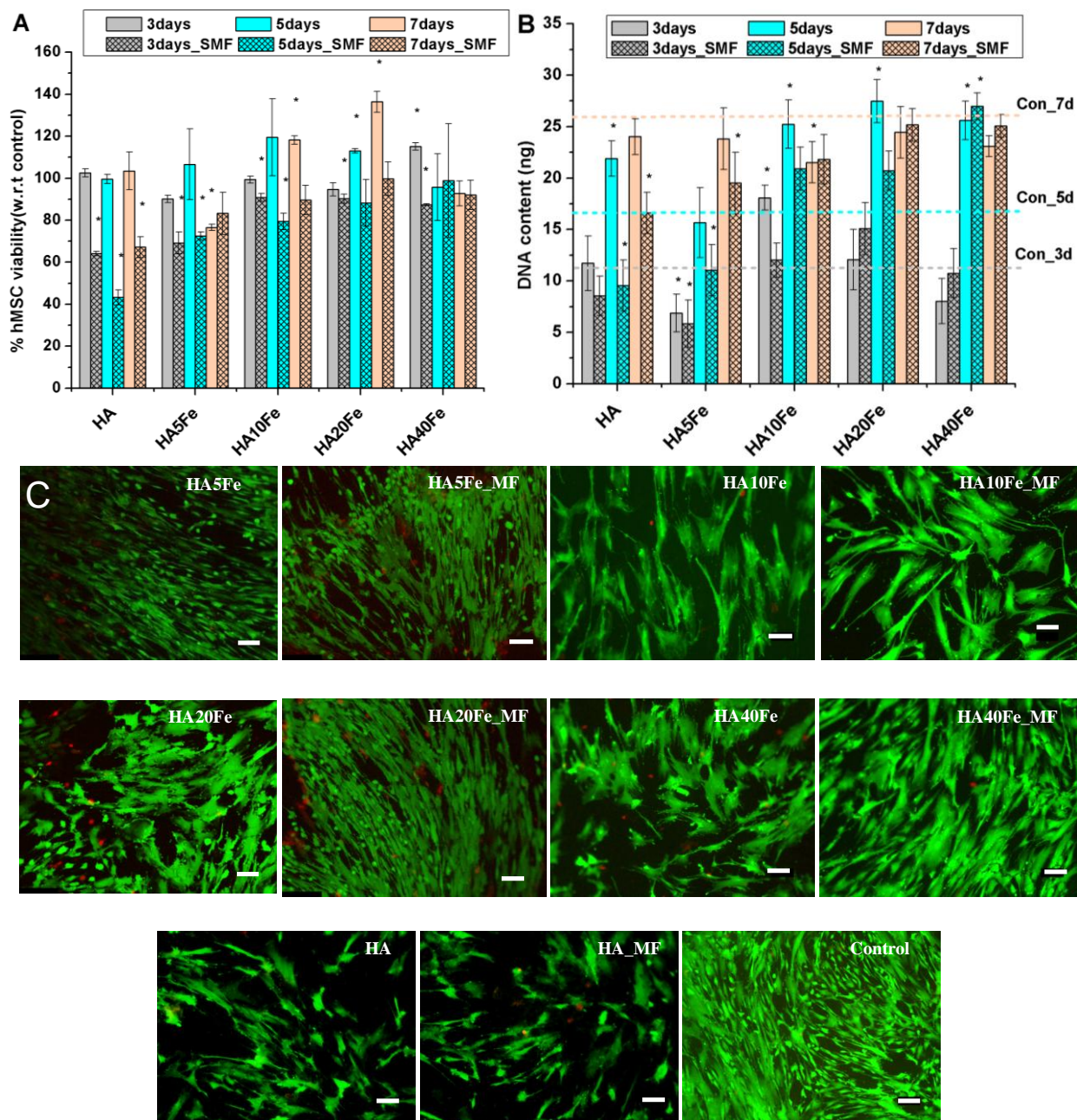


Fig. 5: (A) Viability and (B) proliferation of hMSCs determined by MTT and Picogreen assay respectively, when cultured on HA-xFe₃O₄ magnetic composites and with regular exposure to SMF-100 mT. The dotted lines represent the control data on the corresponding days. Data are represented as mean \pm S.D of n=3 replicates and * represents statistically significant difference at p<0.05 as compared to control. (C) Live/dead staining of hMSCs after 7 days of normal and MF culture. (Green = FDA (live); Red = PI (dead)); Scale bar = 100 μ m.

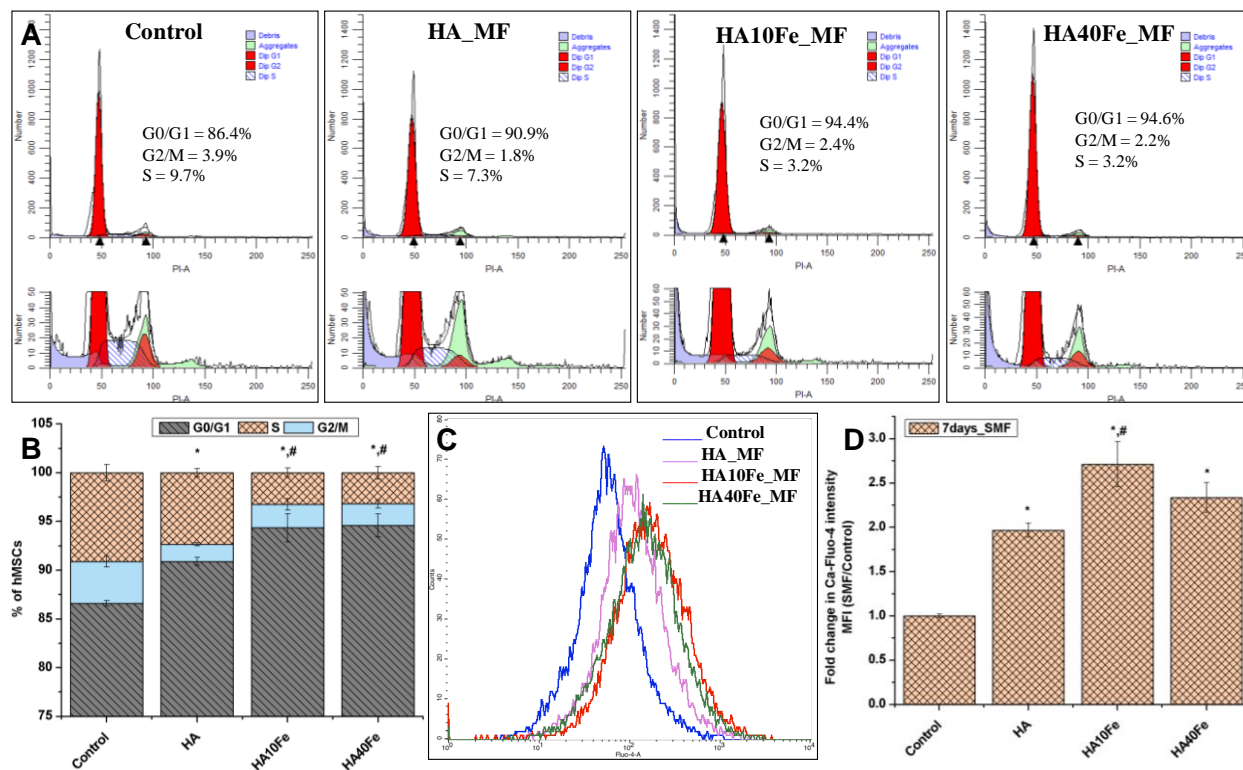


Fig. 6: (A) Representative histogram plots showing hMSC populations in different stages of cell cycle after 7 days of SMF culture on HA- $x\text{Fe}_3\text{O}_4$ composites. The data were fit by Modfit software. (B) Cell cycle analysis of SMF treated hMSCs. (C) Flow cytometric analysis of intracellular calcium levels in SMF exposed hMSCs after 7 days of culture. The data has been represented by an overlay of histograms. (D) Fold increase in intracellular calcium calculated as the ratio of mean fluorescent intensity of the Ca-Fluo-4 complex for SMF to control samples. All data are represented as mean \pm sd of $n=3$ replicates from two independent experiments. * and # indicate statistically significant difference ($p<0.05$) as compared to control and HA, respectively.

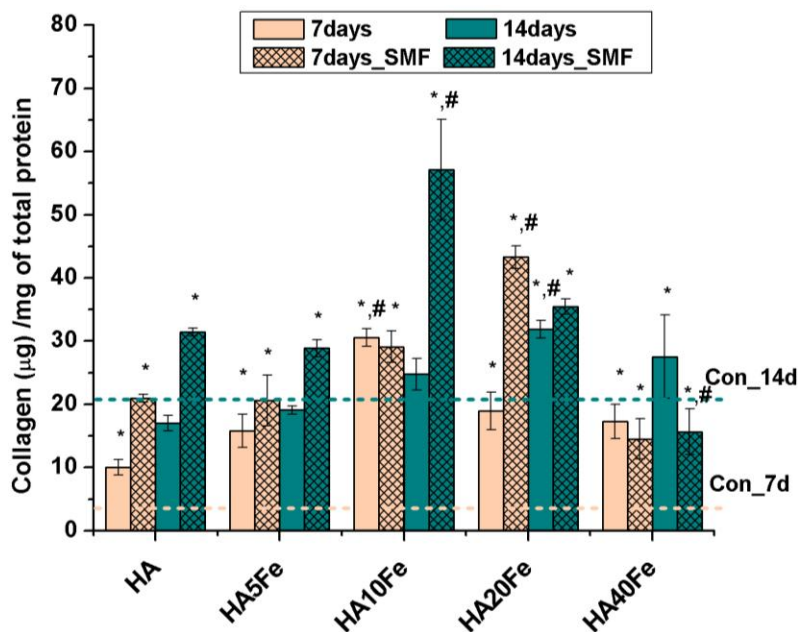


Fig. 7: Bar chart showing the variation in total soluble collagen secreted by hMSCs cultured on HA-xFe₃O₄ composites for 7 and 14 days, without and with MF exposure. The control data are represented by dotted lines. All data are represented as mean \pm sd of n=3 replicates from two independent experiments. * indicates statistically significant difference ($p < 0.05$) as compared to control, while # denotes significant difference ($p < 0.05$) as compared to HA at the same time point.

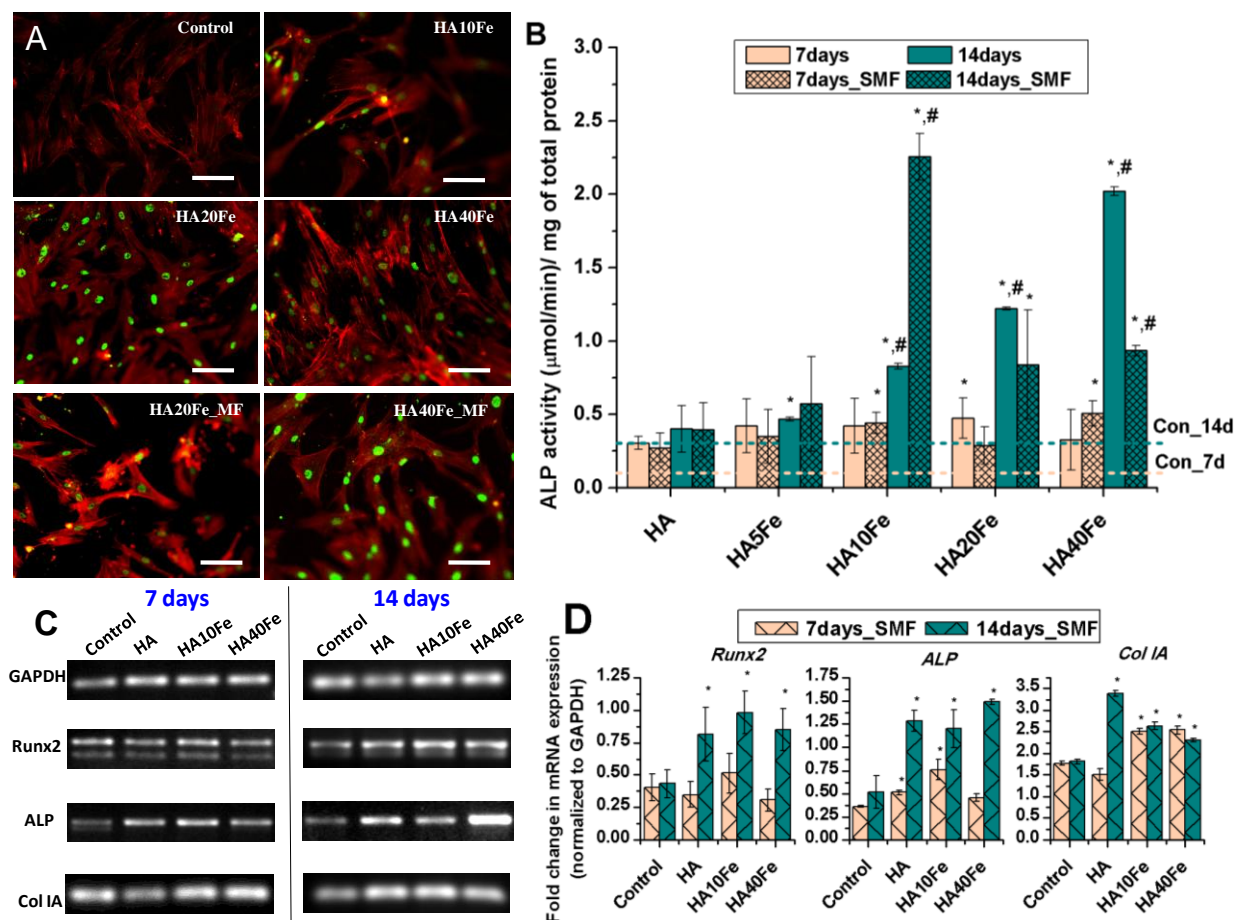


Fig. 8: (A) Fluorescence images of hMSCs showing Runx2 expression in HA-xFe₃O₄ composites after for 5 days of normal and MF stimulated culture. Green nuclei – Runx2 antibody, red – cytoskeleton and scale bar = 100 μm. (B) ALP activity determined biochemically with pNpp substrate after 7 and 14 days of culture. (C) PCR bands for the early osteogenic expression after 7 and 14 days of MF culture and (D) Densitometric analysis of the PCR bands shown in (C) quantifying of the fold change in mRNA expression. All data are represented as mean ± sd of n=3 replicates from two independent experiments. * indicates statistically significant difference (p<0.05) as compared to control, while # denotes significant difference (p<0.05) in comparison to HA at the same time point.

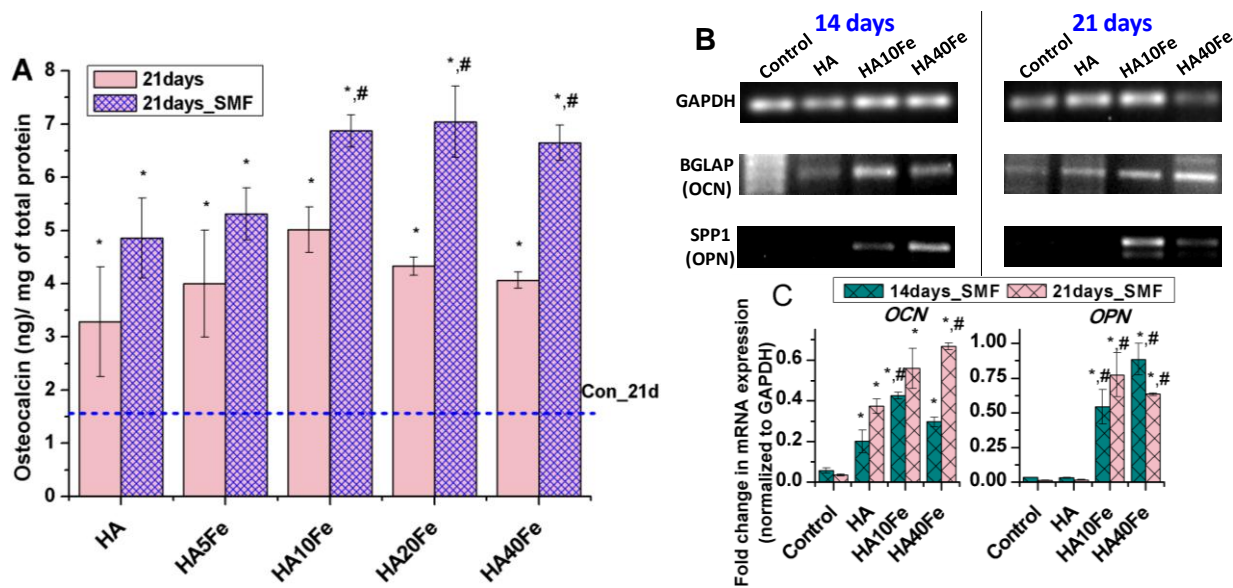


Fig. 9: (A) Human osteocalcin levels determined by ELISA after 21 days of normal and MF culture. The dotted line represents the control (B) PCR bands of late bone marker expression after 14 and 21 days of MF culture and (C) Densitometric analysis of PCR bands in (B) quantifying of the fold change in mRNA expression. All data are represented as mean \pm sd of $n=3$ replicates from two independent experiments. * indicates statistically significant difference ($p<0.05$) as compared to control, while # denotes significant difference ($p<0.05$) in comparison to HA at the same time point.

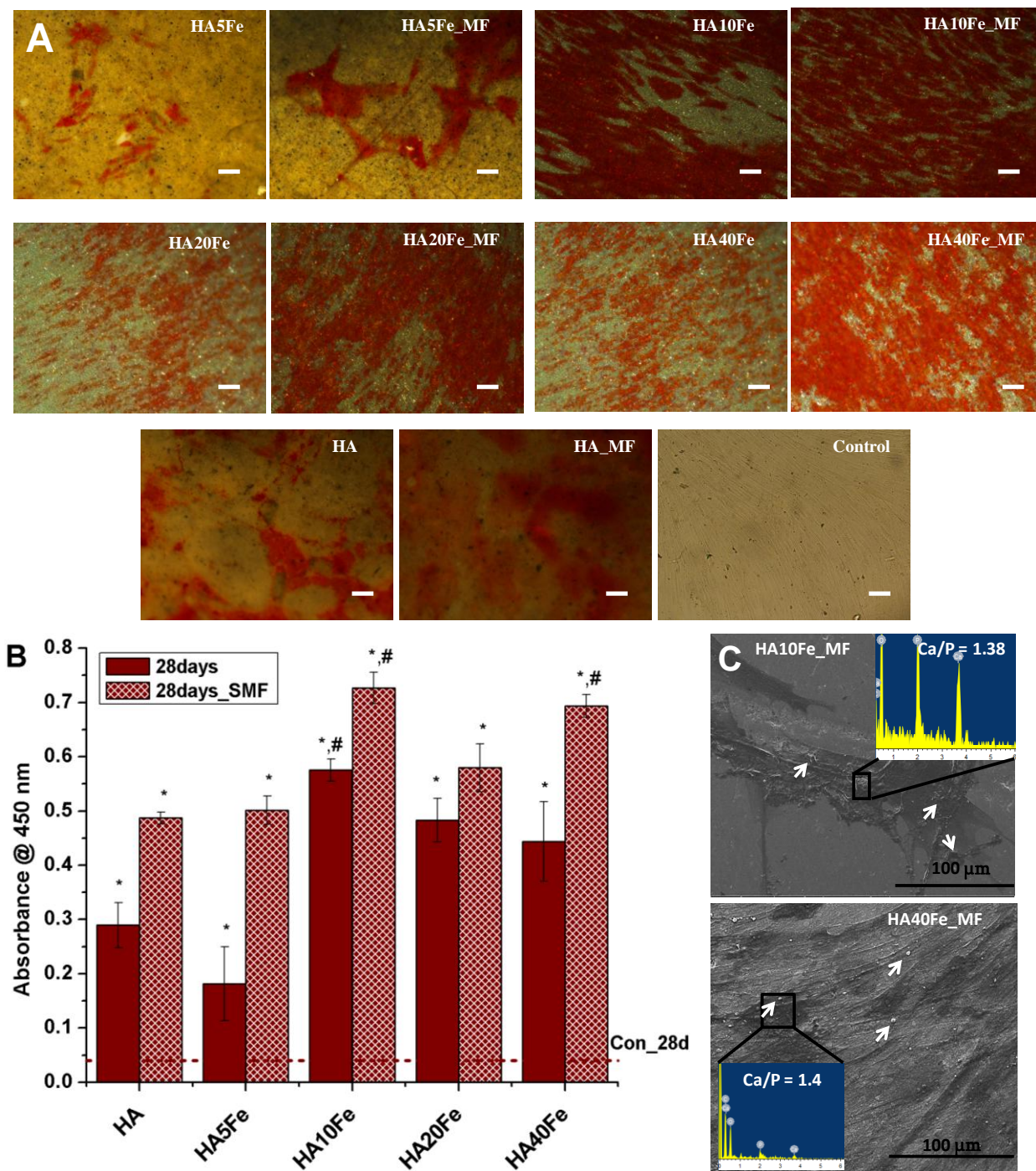


Fig. 10: (A) Alizarin red staining of hMSCs cultured on HA- $x\text{Fe}_3\text{O}_4$ composites for 28 days under normal and MF culture; Scale bar = 100 μm . The dotted line represents the control (B) Quantification of calcium content by detecting absorbance of ARS extracts; All data are represented as mean \pm sd of $n=3$ replicates from two independent experiments. * indicates statistically significant difference ($p<0.05$) as compared to control, while # denotes significant difference ($p<0.05$) in comparison to HA. (C) Representative SEM micrographs along with EDX showing mineralization of CaP nodules after 28 days of MF culture.

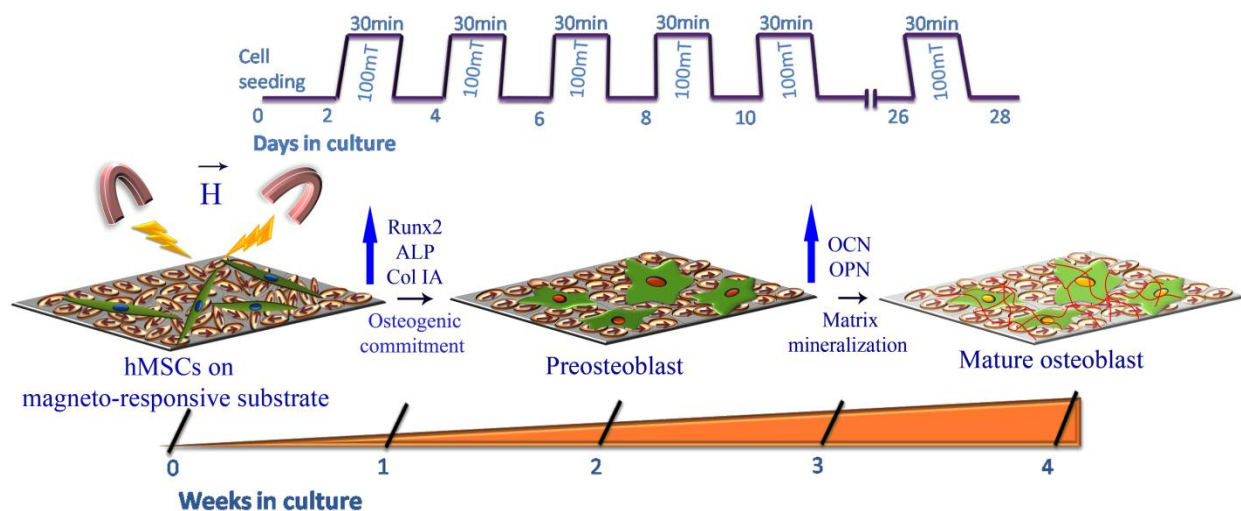
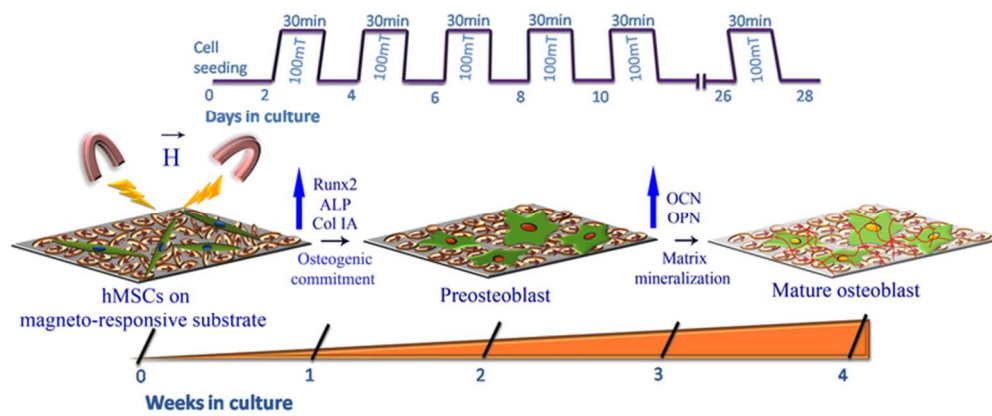


Fig. 11: Substrate magnetization induced osteogenic differentiation of hMSCs cultured on magneto-responsive HA- $x\text{Fe}_3\text{O}_4$ composites in magnetic field stimulated culture conditions.



68x27mm (300 x 300 DPI)